Carbon-based Bifunctional Electrocatalysts for Metal-air Battery Applications

by

Yulong Liu

A thesis

presented to the University of Waterloo

in fulfillment of the

thesis requirement for the degree of

Master of Applied Science

in

Chemical Engineering

Waterloo, Ontario, Canada, 2013

Author's Declaration

I hereby declare that I am the sole author of this thesis. This is a true copy of the thesis, including any required final revisions, as accepted by my examiners.

I understand that my thesis may be made electronically available to the public.

Abstract

The ever-increasing energy consumption and the environmental issues from the excessive rely on fossil fuels have triggered intensive research on the next generation power sources. Metal-air batteries, as one of the most promising technologies emerged, have attracted enormous attention due to its low cost, environmental benignity and high energy density.Among all types of metal-air batteries, Zn-air batteries in particular have tremendous potential for use as alternative energy storage primarily by the low-cost, abundance, low equilibrium potential, environmental benignity, a flat discharge voltage and a longer shell life[1, 2]. However, there are still issues in pertinent to the anode, electrolyte and cathode that remain to be overcome. In particular, the electrocatalyst at the cathode of a metal-air battery which catalyzes the electrochemistry reactions during charge and discharge of the cell plays the most crucial role for the successful commercialization of the metal-air technology.

A series of studies from the carbon nanofibres to spinel cobalt oxide and perovskite lanthanum nickelate was conducted to explore the ORR/OER catalytic properties of those materials which lead to further investigations of the non-precious metal oxide/carbon hybrids as bifunctional catalysts.

Introducing ORR active species such as nitrogen[3], sulfur[4], boron[5] and phosphorus[6] into high surface area carbon has been an effective strategy to fabricate high catalytic activity ORR electrocatalyst. Carbon nanofibre is an abundant, low cost and conductive material that has tremendous potential as ORR catalyst, especially via KOH activation and nitrogen-doping post-treatments. These two post-treatment methods serve as simplistic methodologies to enhance the carbon surface area and ORR catalytic activity of the pristine

carbon nanofibres, respectively. The activated and nitrogen-doped carbon nanofibres demonstrated 26% of improved half-wave potential and 17% of increased limiting current density as a comparison to the pristine carbon nanofibre via RDE testing in alkaline electrolyte. To realize the catalytic activity of activated and nitrogen-doped carbon nanofibres in a more practical condition, they are further evaluated in Zn-air batteries. Polarization curves retrieved from Zn-air cell testing showed 75% higher voltage obtained by activated and nitrogen-doped carbon nanofibres than pristine carbon nanofibres at 70mAcm^{-2} current density.

Structured oxides such as spinels and perovskites have been widely reported as ORR and OER catalyst in metal-air batteries[7-11]. It is widely known that the properties of nanostructures are closely pertinent to their morphologies. The initial performance and durability of cubic Co3O4 synthesized from Feng et al [12]and $LaNiO_3$ from modified sol-gel method are tested in RDE system. After the durability testing, the ORR onset potential and limiting current density of cubic Co_3O_4 has decreased by 50% and 25%, respectively, whereas the OER limiting current density dropped significantly from ~15mAcm2 to almost zero current density. $LaNiO_3$ with different particle sizes synthesized from modified sol-gel method was prepared and evaluated in RDE system. A particle size related performance can be clearly seen from the RDE results. The ORR limiting current of the lanthanum nickelate with smaller particle size (LNO-1) is higher than that of lanthanum nickelate with larger particle size (LNO-0) by 40% and the OER limiting current of LNO-1 is almost tripled that of LNO-0.

With the previous experience on carbon material and structured oxides, two hybrid bifunctional catalysts were prepared and their performance was evaluated. cCo_3O_4/ExNG was made by physically mixing of cCo_3O_4 with ExNG with 1to 1 ratio. The hybrid showed enhanced bifunctional catalytic activities compared to each of its individual performance. Based on the

voltammetry results, a significant positive shift (+0.16V) in ORR half-wave potential and tripled limiting current were observed in the case of the hybrid compared to the pure cobalt oxide. By combing cCo_3O_4 and ExNG, the OER limiting current of the hybrid exceeds that of cCo_3O_4 by ca. 33% and four-fold that of the ExNG. The kinetic current density at -0.4V for cCo_3O_4/ExNG is 15.9 $mAcm^{-2}$ which is roughly 4 times the kinetic current density of the ExNG (3.8 $mAcm^{-2}$) and over 10 times greater than that of cCo_3O_4 (1.1 $mAcm^{-2}$). Electrochemical impedance spectroscopy showed that the charge transfer resistance of the hybrid is ca. one third of cCo_3O_4 and roughly only one half of ExNG which suggests a more efficient electrocatalysis of the hybrid on the air electrode than the other two.

Mixing structured oxides with carbon material provides a simple method of fabricating bifunctional catalysts, however the interactions between those two materials are quite limited. In-situ synthesis of cCo3O4/MWCNT hybrid by chemically attaching $cCo_3O_4$to the acid-functionalized MWCNT is able to provide strong interactions between its components. Through RDE testing, the ORR activity of cCo_3O_4/MWCNT outperformed its individual component showing the highest onset potential (-0.15V) and current density (-2.91 $mAcm^{-2}$ at -0.4V) with ~4 electron transfer pathway. Moreover, the MWCNT and cCo_3O_4 suffered from significant OER degradation after cycling (92% and 94%, respectively) whereas the hybrid material demonstrated an outstanding stability with only 15% of performance decrease, which is also far more superior to the physical mixture (30% higher current density).

Among all the catalyst studied, cCo_3O_4/MWCNT has the highest performance and durability. The excellent performance of the hybrid warrants further in-depth research of non-precious metal oxide/carbon hybrids and the information presented in this thesis will create

afoundation for future investigation towards high performance and durability bifunctional electrocatalysts for metal-air battery applications

Acknowledgements

The work reported herein was financially supported by the Natural Sciences and Engineering Research Council of Canada (NSERC), the University of Waterloo and the Waterloo Institute for nanotechnology.

The author would like to thank Dr. Zhongwei Chen, and Dr. Michael Fowler for their guidance and tremendous assistance throughout the Master's study.

Besides my advisors, I would like to thank the rest of my thesis committee: Prof. Aiping Yu and Prof. Boxin Zhao for their encouragement and insightful comments.

Special thanks goes to the author's colleagues including, Drew Higgins, Jason Wu, Dong Un Lee, Joseph Bae Jung Kim, Brian Kihun Kim, Hey Woong Park, Ligang Feng, Rongyue Wang, Jinyun Liao, Jordan Scott, Ja-Yeon Choi, Zhu Chen, Victor Chabot, Fathy Hassan, Hadis Zarrin, Md Ariful Hoque for their assistance and support. My time spent with all of you was memorable and delightful.

Last but not the least, I would like to thank my uncle Tong Zhang, auntJi Zhou and cousin Yuxi Helena Zhang for their considerate help while my stay in Canada. I would like to thank my family, mom Yibing Zhang and dad Guoyong Liu for giving me so much love and support throughout my life. Without you, I would not have gone this far of my life and I would not have been the person I am now. Whenever I feel exhausted and depressed, I could always remember my home, the spiritual shelter of mine waits for me across the ocean.

Table of Contents

List of Figures

List of Tables

List of Abbreviations

Abbreviation	Description
ORR	Oxygen reduction reaction
OER	Oxygen evolution reaction
Zn-air	Zinc-air
Li-air	Lithium-air
PEMFC	Proton exchange membrane fuel cell
SEM	Scanning electron microscopy
TEM	Transmission electron microscopy
XRD	X-ray diffraction
XPS	X-ray photoelectron spectroscopy
TGA	Thermogravimetric analysis
RDE	Rotating disc electrode
CV	Cyclic voltammetry
EIS	Electrochemical impedance spectroscopy
SCE	Saturated calomel electrode
OCV	Open circuit voltage
GO	Graphite oxide
ExNG	Exfoliated and nitrogen-doped graphene
cCo_3O_4	Cubic cobalt oxide
DDI	Distilled de-ionized water
Pt/C	Platinum supported on carbon
MWCNT	Multi-walled carbon nanotube
CNF	Carbon nanofibre
NCNF	Carbon nanofibre nitrogen-doped at 850˚C
a(950)-CNF	Carbon nanofibre activated at 950 ˚C
a(850)-NCNF	Carbon nanofibre activated at 850˚C and nitrogen-doped at 850˚C

a(950)-NCNF	Carbon nanofibre activated at 950˚C and nitrogen-doped at 850˚C
a(1050)-NCNF	Carbon nanofibre activated at 1050˚C and nitrogen-doped at 850˚C
LNO-0	Lanthanum nickelate with no addition of Vulcan carbon
LNO-1	Vulcan carbon addition ratio 1:1 the theoretical $LaNiO_3$ yield
LNO-2	Vulcan carbon addition ratio 2:1 the theoretical $LaNiO_3$ yield
LNO-3	Vulcan carbon addition ratio 3:1 the theoretical $LaNiO_3$ yield
cCo_3O_4/MWCNT	Cubic cobalt oxide/multi-walled carbon nanotube

CHAPTER 1: Introduction

1.1 Motivation and Objectives

Currently, over 80% of the energy for the human society was supplied from non-renewable fossil fuels[13], which come with associated environmental impacts and rapid resources depletion. The use of energy storage systems, specifically batteries, will reduce the environmental impacts and provide sustainable power sources

Zn-air is an emerging battery (or fuel cell) technology that offers inexpensive energy solution while simultaneously providing large storage capacity and energy generation.It was considered as promising candidates ranging from portable electronic devices to large scale grid energy storage. However, cost is one of the key barriers for the successful commercialization.Conventionally, precious metal was adopted for catalyzing the oxygen reduction reaction (ORR) reactions during the battery discharge but due to the high cost of the precious metaland the limited reserve, development of efficient, durable and low-cost electrocatalyst for Zn-air battery application is extremely desirable.

The current challenges of the cathode electrocatalysts in a metal-air cell reside in the high fabrication cost of the electrocatalyst. In order to be able to reach satisfactory performance of the battery, conventionally precious metals or metal oxides are adopted to catalyze the oxygen reduction reactions (ORR) for discharging and oxygen evolution reactions (OER) happened during charging of a cell. But these state-of-the-art catalysts are too expensive for large-scale implementations which inhibit the commercialization of metal-air batteries. As a result, non-

precious catalysts aiming to replace the state of the art precious catalysts have been intensively studied.

In this thesis, non-precious electrocatalysts for ORR and OER reactions are synthesized and characterized. Carbon materials represent one of the most studied catalysts or supports for oxygen reduction reactions. Among them, carbon nanotubes, carbon nanofibres and graphene are those of most studied and generally ORR active species were introduced into their structures to improve their ORR activities. Non-precious metal oxides represent another category of catalysts for metal-air battery applications and structured oxides like spinels and perovskites have been widely reported to be active catalysts for both ORR and OER. However, preparation of those spinels and perovskites by traditional sol-gel methods gives particles of large size and therefore smaller surface area. New methodologies for smaller particle size and larger surface area used for synthesizing these materials as ORR and OER electrocatalysts are expected to enhance the performance. Since spinles and perovskites are semiconductors and good catalytic activities require fast electron transport, the attachment of those metal oxides onto a conducting surface, preferably a carbon surface would further enhance their activities. As a result, non-precious metal oxide/carbon hybrids are expected to have ORR/OER bifunctional catalytic activities that potentially exhibit superior performance to either component of the hybrid.

The objective of this work is to explore the possibility of replacing the state-of-the-art ORR electrocatalysis (Pt/C) by non-precious microstructured and nanostructured electrocatalysts for primary Zn-air battery applications and based upon that, synthesizing novel bifunctional catalysts which are able to catalyze both ORR and OER reactions for rechargeable Zn-air battery applications.Four different catalysts have been developed in this work:

- Activated and Nitrogen-doped Carbon Nanofibres
- Spinel Cobalt Oxide and Perovskite Lanthanum Nickelate
- Cubic Spinel Cobalt Oxide/Exfoliated and Nitrogen-doped Graphene
- Cubic Spinel Cobalt Oxide/Multi-walled Carbon Nanotubes

The work reported here is to target the lack of affordable, efficient and durable bifunctional catalyst from preliminary research on carbon material (CNFs) and structured metal oxides (Co_3O_4 and $LaNiO_3$) to the hybrid bifunctional catalysts based upon the previous experience. An initial overview of the metal-air battery technology including details on operation principles, technical challenges within the cell and the current development of electrocatalysts for Zn-air batteries will serve as a foundation for the discussion on the studied catalyst development and evaluation. Experimental methods on synthesizing the studied catalysts will also be described followed by a detailed discussion of their performance as either ORR or OER catalyst, or as bifunctional catalysts. The thesis will be ended with a summary of research findings along with some potential recommendations and improvement of the conducted experiments.

1.2 Introduction to Metal-air Batteries

The system configurations of metal-air batteries lie in between conventional batteries and fuel cells. A conventional battery is a closed electrochemical system that converts chemical energy directly into electrical energy with a fixed supply of reactants[14]. A primary battery is a cell, or group of cells, that discharges during operation and is discarded when the electrical energy to be used is exhausted[15]. Secondary batteries, or rechargeable batteries, can be discharged and then returned to their original condition via charging[14]. This differentiates themselves from primary

batteries, which cannot be restored to their full charged condition after discharge.In contrast to the closedsystem configurations of batteries, a fuel cell is an open electrochemical conversion device that continuously generates electric energy as long as fuels are supplied[16].The system configurations of metal-air batteries is essentially a fuel cell/battery hybrid[17]. In this respect, metal-air batteries are often called metal-air fuel cells. This featured open cell structure provides metal-air batteries with relatively high specific power and specific energy. As shown in Fig. 1, Zn-air batteries, for instance, demonstrate a higher peak power than hydrogen fuel cells and batteries such as Ni/Zn and Pb-lead batteries whereas its specific energy shows higher value than the Ni/Zn, Pb-lead and lithium-ion batteries but lower than hydrogen fuel cells. Primary metal-air batteries are able to generate electricity by consuming the stored metal at the anode and oxygen from the ambient atmosphere through the open cathode. Although not fully electrically rechargeable at present, metal-air batteries such as Zn-air, Al-air and Mg-air batteries may be recharged mechanically by replacing the consumed anode and spent electrolyte with fresh metal and electrolyte[18]. Though this operation could be effective in limited applications, there is a need to develop electrically rechargeable metal-air batteries in some applications such as energy storage devices. Like other battery and fuel cell technologies, metal-air batteries also suffer from a series of technological and scientific issues that will be discussed in section 1.2.2 in detail.

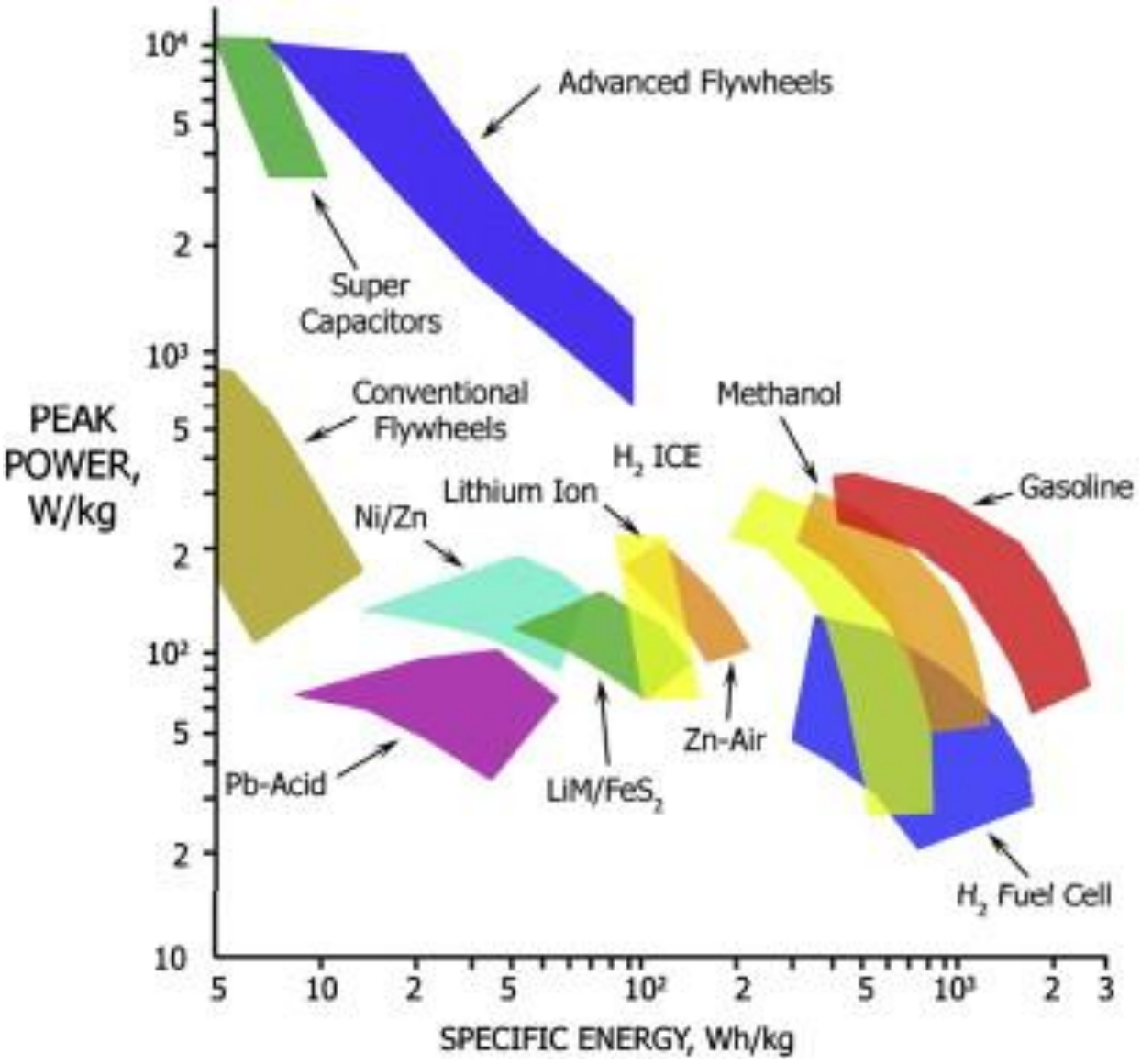

Fig.1. The Ragone plot, comparing the energy and power density of different energy sources[19].

The concept of metal-air batterieshas been known for more than hundred years. The first metal-air battery was constructed by Lechanche in 1868 with carbon supported manganese dioxide as air electrode. In 1932, Schudmacher and Heise came up with a more modern design of a metal-air battery[20]. The metal-air battery is an attractive energy storage and generation device because of the decreased weight, volume and cost that can be achieved by using the

oxygen in the atmosphere as the source of cathode reactant. Although the metal-air battery technology originates from the 19th century, metal-air batteries were first put into commercialization in the beginning of the 20th century as primary button cells. The two types of metal-air batteries commonly investigated are primary and secondary. In the past few years, the increasing global energy demand along with the depletion of fossil fuels has triggered intensive research on alternative energy supplies and energy storage devices. This has encouraged the scientific community to revisit metal-air battery technologies and solve issues that has impeded their large-scale implementations.

Several metal-air chemistries have been studied with the aim of realizing the potential of metal-air batteries. In the past, Li, Al, Mg, Zn- air cell chemistries emerge owning to the outstanding specific capacities of these anode materials (3842mAh/g for Li, 2965mAh/g for Al, 2204mAh/g for Mg vs. 815mAh/g for Zn[21]). Besides their high specific capacities, the use of earth abundant metals as anode materials makes the metal-air technology much cheaper than the fuel cell technology. Utilizing alkaline electrolyte createsa more durable environment for the cathode eletrocatalystthan the acidic electrolyte adopted in polymer electrolyte membrane fuel cells (PEMFCs)which allows a broader selection of oxygen catalysts, especially for non-precious bifunctional catalysts[22].Additionally, the advantageous design of metal-air batteries, where using oxygen from the air as the cathode oxidants, allows the battery to be filled with more of the anode materials, which significantly increase the energy density of the system.

According to the electrochemical equivalent of metal, the principle advantage of using lithium metal in the metal-air battery is its high theoretical specific energy of 13124 Whkg^{-1}and high theoretical battery voltage of 3.4 V which is the highest among all types of metal-air batteries. However, lithium-air battery is still in the infancy of development whereby the

irreversible loss of capacity in organic electrolyte and the lack of stable air electrode materials along with metal availability, cost, and safety concerns[18, 23-25], and furthermore, the fundamental mechanisms are not yet fully understood[26, 27] and lithium has significant safety issues when used as a pure metal electrode. Calcium, magnesium, and aluminum have also attracted attention due to their highly energy dense nature. Nevertheless, high cost and problems regarding anode polarization, instability, safety and parasitic corrosion have prohibited the development of commercial products[17, 18, 28], albeit magnesium-air and aluminum-air battery have found some military applicationsand exploration for underwater propulsion[28].

Among various types of metal anode studied over years, zinc was the first metal commercially implemented amongprimary metal-air batteries Fig 2. It is abundant, relatively inexpensive, and stable in aqueous alkaline electrolytes.Primary Zn-air batteries are cheap, easy to handle and environmentally friendly. The Zn-air battery technology is the most mature one of its type[29]. Zn-air button cells were actively developed 40 years ago. In 1970's, Zn-air button cells suffered from electrode leakage issues. After decades, the new design of Zn-air cell successful made Zn-air button cells available for use in hearing aids by the mid- 70's and Zn-air cells became the standard for hearing aid applications by the mid 1980's[30]. The successful commercialization of primary zinc-air cells sets a strong foundation for further research and development as secondary batteries. Nevertheless, enormous efforts are stillrequired to overcome some significant drawbacks limiting this technology which will be discussed in the following section with great details.

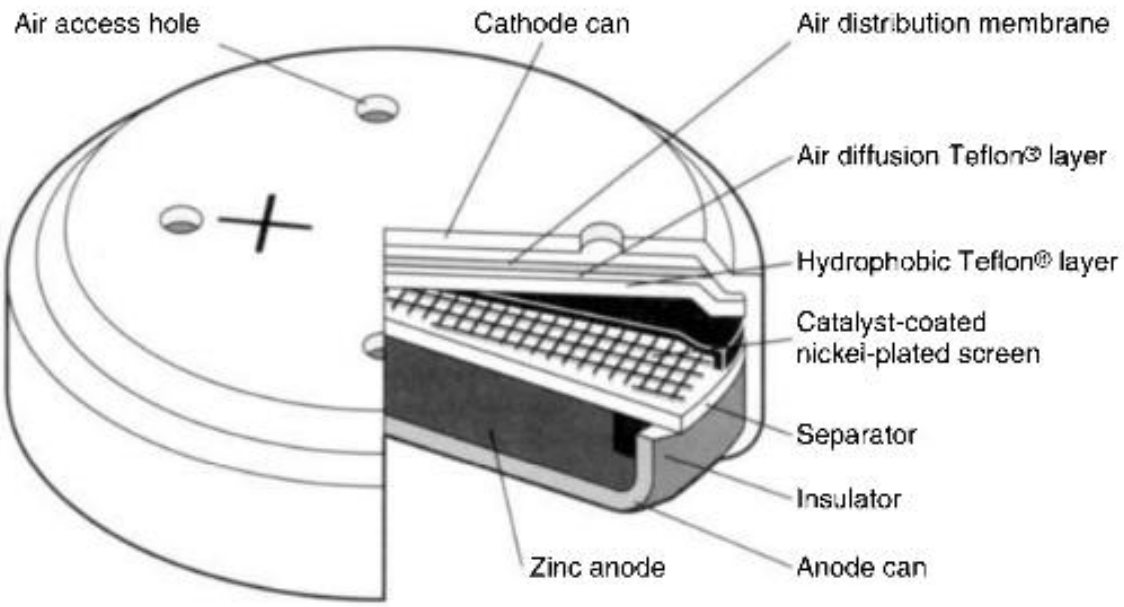

Fig.2. Typical Zn-air button cell (components not to scale) (Courtesy of Duracell, Inc.)[31]

1.2.1 Operation Principles of Metal-air Batteries

Establishing an understanding of the fundamental reaction mechanisms of metal-air batteries is an essential aspect in the design of rechargeable systems. Two electrochemical half-reactions constitute the energy conversion in a metal-air battery which is the reduction of oxygen at the cathode and the oxidation of metal at the anode. The oxygen reduction reaction is an important cathode reaction for a range of energy applications in fuel cells[32-34], metal-air batteries[3, 35] and chlor-alkali electrolysis[36]. The strong O=O double bond present in oxygen molecules makes oxygen reduction reactions difficult to proceed which requires the transfer of four coupled electron and proton[37]. The oxygen reduction reaction taking place at the cathode during the battery discharge can be written as the following,

$$O_2 + 2H_2O + 4e^- \leftrightarrow 4OH^- E^0_{cathode} = +0.401V \qquad (1)$$

In Equation 1, e^- denotes electron and E^0 denotes the theoretical half-cell voltage calculated based onthermodynamic data at standard conditions. This reaction happened by consuming the oxygen from ambient air leaving the primary mass in the metal-air battery the metal electrode which is oxidizes during battery discharges according to the below reaction,

$$M \rightarrow M^{n+} + ne^- E^0_{anode} = depend\ on\ the\ metal \qquad (2)$$

In Equation 2, M denotes the specific metal utilized in a particular metal-air battery system, and the number n depends on the valence electron of the specific metal in consideration. Evidently, the theoretical half-cell voltage is specific to the selection of metal in this reaction. The theoretical battery voltage can be calculated by the following equation,

$$E^0_{battery} = E^0_{cathode} - E^0_{anode} \qquad (3)$$

In the case of energy storage in the metal-air battery, the reverse reaction of the oxygen reduction reaction, oxygen evolution reaction takes place by the reverse reaction of the Equation 1. As the reverse reaction of oxygen reduction reactions, oxygen evolution reactions also proceed via multistep proton-coupled electron transfer processes and are kinetically sluggish[38, 39]. During oxygen evolution reactions, the reaction happened on the metal is also reversed from the oxygen reduction reactions. It should be noted that under this scenario, the cathode and anode reverses during battery charge operation. Under such condition, the metal electrode becomes the cathode, and the air electrode becomes the anode. Table 1 shows the theoretical open circuit voltage (OCV), practical OCV and theoretical specific energy of metal-air batteries with various anode metals.

Table 1 Comparisons of different metal-air battery anodes

Metal	Theoretical OCV (V)	Practical OCV (V)	Theoretical Specific Energy (kWh/kg)	Reference
Li	2.9-3.1	~2.5	11500	[40]
Al	2.78	~2	8100	[41]
Zn	1.65	1.46	1350	[42]
Fe	1.3	N/A	960-1200	[43]

Of different types of metal-air batteries, the primary Zn-air battery has been successfully commercialized as hearing-aid batteries. One typical Zn-air battery consists of three main components shown in Fig. 1: zinc anode, electrolyte and the air cathode. For a compact design, the use of a separator is necessary. The overall Zn-air chemistry is described as the following[44],

$$Anode: Zn + 4OH^- \rightarrow Zn(OH)_4^{2-} + 2e^-$$

$$Electrolyte: Zn(OH)_4^{2-} \rightarrow ZnO + H_2O + 2OH^-$$

$$Cathode: \frac{1}{2}O_2 + H_2O + 2e^- \rightarrow 2OH^-$$

$$Overall: 2Zn + O_2 \rightarrow 2ZnO$$

Essentially, during discharge, oxygen is reduced at the porous air electrode by the eletrocatalyst into hydroxide ion OH^-. The hydroxide ions combined with the zinc ion generated from the oxidation of zinc metal to form the aqueous soluble zincate ion $Zn(OH)_4^{2-}$[17]. Concurrently, the electrons generated from the oxidation of zinc metal provide electricity. When

the zincate ion $Zn(OH)_4^{2-}$ reaches its saturation point, they will precipitate out the solution in the form of zinc oxide ZnO, which completes the whole discharge process. Accordingly, by reverse the discharging process, theoretically the Zn-air battery can be electrically charged. However, electrically rechargeable Zn-air battery currently remains at research and development level. Albeit not be able to full electrically recharged, Zn-air battery may be recharged mechanically by replacing the consumed zinc anode and replenish the electrolyte[17, 18, 45].

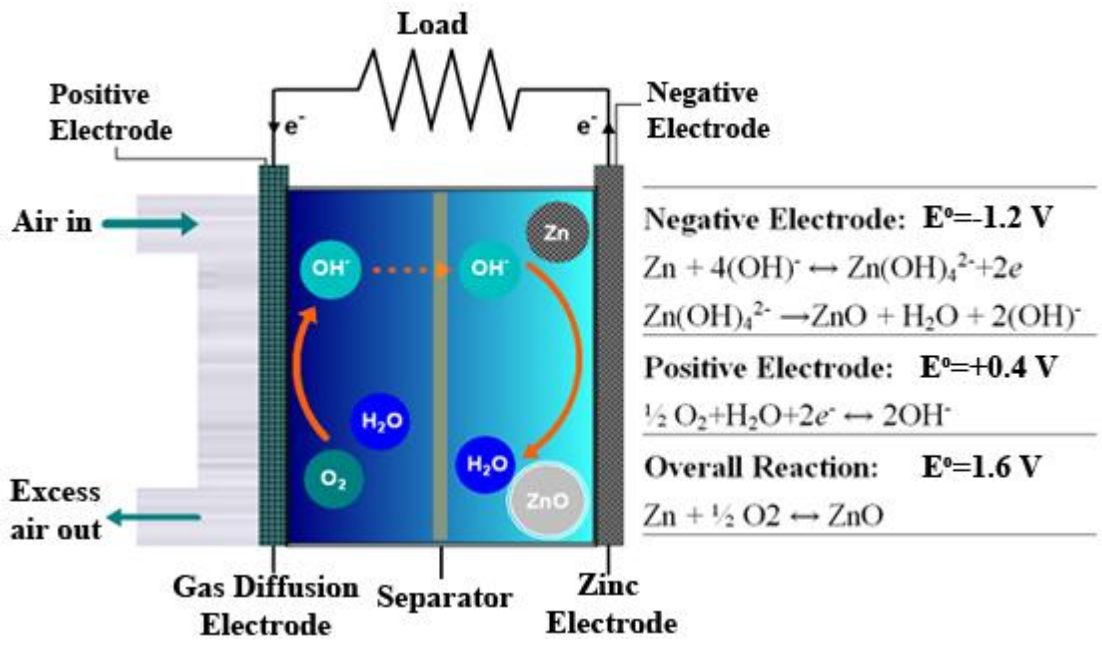

Fig.3. Schematics of a typical Zn-air battery[46]

1.2.2 Technical Challenges

1.2.2.1 Component of Zn-air Battery – the Anode

The important criteria for a good battery anode are as the following [47]:

(1). High negative OCV in the electrolyte under consideration;

(2). Negligible corrosion rate;

(3). Minimum electrode polarization;

(4). High material utilization efficiency (high surface area in most cases);

(5). Minimal environmental burden;

(6) Low cost

Considering the case of Zn-air battery, zinc metal is a low cost and environmentallybenign material. Unlike aluminum and other metal-air battery anode materials, zinc will corrode only slowly when immersed in alkaline electrolyte. All the above-mentioned characteristics of zinc metal make it an excellent candidate for metal-air battery application. However, zinc metal still faces several issues that require in-depth research to realize the technology's potential.

Typical Zn-air batteries utilize pure zinc metal as the active mass at the anode. The current challenges at the zinc anode are the low utilization of the anode metal, low hydrogen evolution overpotential and the formation of zinc dendrite formed during the charging of the cell. These issues must be overcome before the successful commercialization of electrically rechargeable Zn-air battery.In order to increase the utilization of zinc metal, various morphologies of zinc metal such as zinc particles[48], zinc dendrites[48], and zinc fibres[49] have been reported aiming to maximize the contact surface area between the zinc and the electrolyte. Alloying zinc metal with other metals has also been reported to increase the zinc metal utilization[42, 50]. Hydrogen evolution reaction is a process to produce hydrogen gas. Compared to the oxygen reduction/evolution reactions, hydrogen evolution reaction only involves two electron transfer affording faster reaction kinetics[51]. As a result, the low

hydrogen evolution overpotential of zinc metal lays a potential risk when a Zn-air cell is under operation due to the hydrogen gas accumulation within the cell. Several authors [50, 52-54]have investigated the ability of additives (surfactants, alloys) to suppress hydrogen evolution on zinc electrodes. Others reports in the literature the addition of lead oxide into the anode material successfully raise the hydrogen overpotential[55]. Compared to the low utilization and hydrogen evolution overpotential of the zinc metal, the formation of dendrite is a greater challenge that prohibits the successful development of rechargeable Zn-air battery with compact design. For rechargeable Zn-air cell, the zinc metal is consumed during discharging and regenerated during charging. Along with this process, zinc dendrites are formed, where zinc builds unevenly in the form of branch-like structure (Fig.3) that can penetrate the separator and short-circuit the cell[1]. Various approaches have been reported aiming to solve this issue by means of zinc alloying[56] or the addition of additives into the zinc anode[55, 57].

Fig.4. The electrolytic dendritic-zinc powder[48]

1.2.2.2 Component of Zn-air Battery – the Electrolyte& Separator

The types of electrolyte employed in Zn-air batteries fall into two categories: the liquid electrolyte and solid electrolyte. Aqueous potassium hydroxide electrolyte is commonly adopted in Zn-air battery. Compared with using aqueous sodium hydroxide, potassium ions have superior ionic conductivity 73.50 $\Omega^{-1}cm_2$/equivalent[58]. With respect to potassium hydroxide aqueous solution concentration, lower concentration reduces the amount of ions available for reaction and increases electrolyte resistance; on the other hand, high salt concentration leads to high viscosity which retards ion transport and therefore may lead to oxygen transport pathway blockage. The ionic conductivity of potassium hydroxide aqueous solution reaches its maximum at

6Mpotassium hydroxide concentration.Although the aqueous electrolyte is easy to prepare and gives high ionic conductivity, issues such as potential leakage[59], carbonate formation from CO_2 in the air[59] and high sensitivity to temperature and humidity hinder the large-scale commercialization of Zn-air battery technology. Aiming to overcome these issues, the solid electrolytes are an emerging research area whereby OH^- transportation is assisted by the functional groups present on the polymer chains. Nevertheless, tremendous efforts are still required to enhance the ionic conductivity and stability.

The separator is a crucial component in Zn-air batteries with compact design which is utilized to separate the anode and cathode from short circuit. The separator also requires proper porosity to allow OH^- to pass through without much resistance in order to complete the electrochemistry meanwhile preventing the air cathode blockage from the zinc ions migration.In some scenarios, the concepts of a separator and a solid electrolyte are used interchangeably due to their function similarities. The commercial Zn-air cells use laminated separators such as Celgard 4560 and Celgard 5550, which have a microporous membrane laminated with a nonwoven[60]. Besides the commercialized Celgard membranes, new types of Zn-air battery separators have been developed. Wu et al. applied sulfonation method on the commercial Celgard 2320 membrane resulting in an increased hydroxide conductivity and hydrophobicity[61]. Dewi et al. adopted a cationic polysulfonium membrane as a separator in a Zn-air cell which provided high efficiency in preventing zinc cation migration to the cathode[62].

1.2.2.3 Component of Zn-air Battery – the Cathode

In contrast to the conventional battery electrode, the active mass of the electrochemistry reactions was drawn from the ambient air by employing porous air cathode. The electrochemistry at the cathode takes place at the triple phase boundary where the electrocatalyst, electrolyte and the oxygen are in contact. Consequently, an excellent design of an air cathode will be able to maximize the area of triple phase boundary Fig. 5.

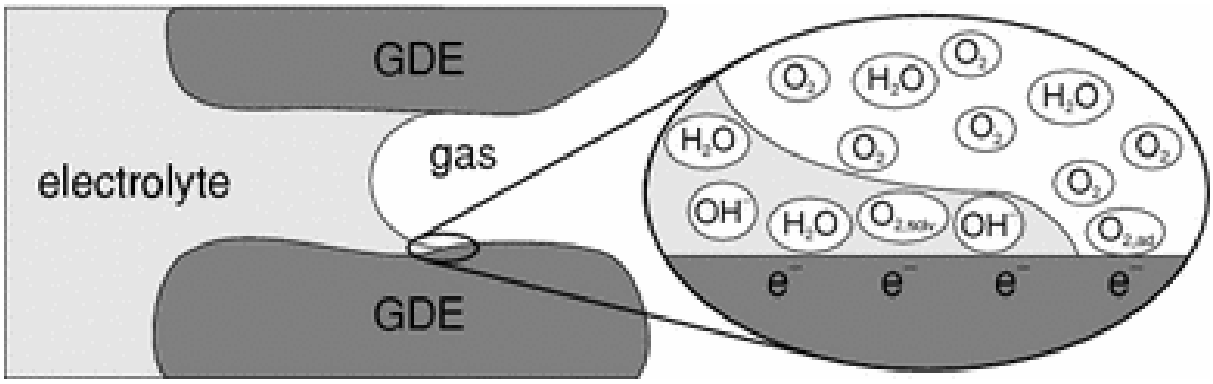

Fig.5. Oxygen reduction at triple phase boundary in oxygen cathodes[36].

A typical air cathode consists of three components, a catalyst layer, a gas diffusion layer and a current collectoras shown in Fig. 6. A gas diffusion layer is an integration of several types of carbonaceous materials bound together by polytetrafluoroethylene (PTFE) followed by burning off the PTFE which results in a porous structure. Depending on the exact nature and use of diffusion media, PTFE can also charge the surface wetting characteristics. The carbon nature and porous structure of gas diffusion layer promotes the air transport and prevents electrolyte from penetrating the gas diffusion layer through pores due to its hydrophobicity.

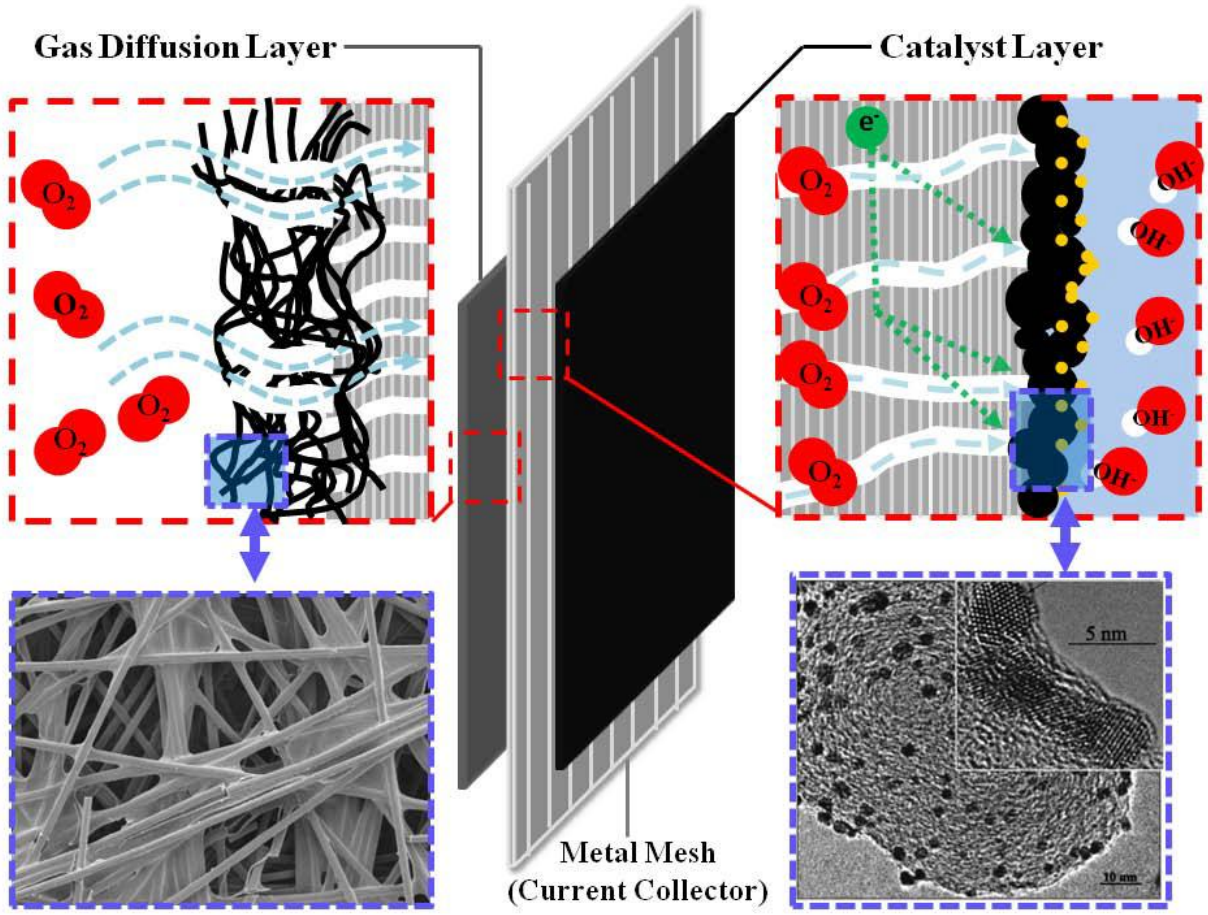

Fig.6. Structure and function of a typical air electrode for Zn-air batteries[46]

The catalyst layer coated onto the gas diffusion layer is the most essential component of the air cathode. Without the electrocatalyst, the oxygen molecules will not be reduced and unable to participate in the electrochemical reactionsdue to the strong O=O bonding.An oxygen reduction reaction is very complex and involves with multiple molecular adsorption-desorption processes. An efficient ORR catalyst is able to catalyze the oxygen reduction process via a four electron transfer mechanism according to Equation 1. For a less efficient ORR catalyst, two electron transfer pathway is usually preceded and can be written as the following which involves the formation of hydroperoxide ion HO_2^- as an intermediate,

$$O_2 + H_2O + 2e^- \leftrightarrow HO_2^- + OH^- E^0 = -0.065V \qquad (4)$$

The HO_2^- can be further reduced to give hydroxide ions according to the following equation,

$$HO_2^- + H_2O + 2e^- \leftrightarrow 3OH^- \qquad E^0 = 0.867V \qquad (5)$$

The two electron transfer mechanism presents a large overpotential that retards the kinetics of oxygen reduction process compared with the four electron transfer pathway. The number of electron transfer is adopted to evaluate the performance of ORR electrocatalyst through Koutecky-Levich plot which will be discussed in detail in section 2.2.2.1. As the reverse reaction of ORR, OER is also sluggish in nature[38, 39]. An effective electrocatalyst is needed to expedite the reaction, reduce the overpotential and therefore increase the energy storage efficiency.

1.2.3 Market of Zn-air Batteries

Zn-air is an emerging battery technology as the next generation energy storage and conversion device. A study of 2008 from Frost & Sullivan revealed the market for Zn-air battery to be $ 251.1 million and a report of 2012 by global industry analysts, Inc. predicted the global market for Zn-air batteries to reach $400.8 million by 2017 driven by environmental concerns, technological innovations and consumer awareness world-wide. Other applications catapulting the rapid growth of Zn-air battery market are back-up power devices, stationary and portable home power generators, mobile electronic devices, grid scale energy storage devices and electric vehicles[1, 2, 17, 63, 64].

Characteristics of Zn-air battery technology such as low operation risk, environmental friendly, low cost make it an outstanding candidate for grid scale energy storage and electric vehicle propulsion. Renewable natural power sources such as photovoltaics and wind turbines are able to be utilized to generate energy. Nevertheless, these energy sources are intermittent and fixed in space which makes them difficult to match the pattern of energy demand. Grid energy storage by electrochemical devices is one method of adapting the energy production to energy consumption that either varies over time. Electrochemical storage devices are able to facilitate the use of intermittent energy sources by the storage of surplus energy during off-peak period and release of the stored energy under peak hours [65, 66]. This would allow the grid be more efficient, reliable and lower cost. Large scale grid energy storage demands the integrated electrochemical devices with long cycle life, low maintenance and high efficiency. According to Table 2, Zn-air batteries satisfy the criteria for grid energy storage with one of the lowest cost. Energy storage and generation devices are under actively explored for electric vehicle applications aiming to consume less gasoline and reduce greenhouse gas emission[67, 68]. For the successful commercialization of such electric vehicles, the energy generation and storage devices require several characteristics such as safety, durability, maintenance cost and the ability to produce desired current density.Zn-air batteries serve as excellent candidates for propelling electric vehicles[69, 70]. Compared to the commercially available fuel cell powered electric vehicles, Zn-air powered electric vehicles cost the least with the highest output voltage and peak operating efficiency as shown in Table 3.

However, despite many advantageous characteristics of Zn-air batteries possess intensive research and development is still required to implement Zn-air battery for various applications.

Table 2 Various types of energy storage for electric [Courtesy of EPRI][71].

Technology option	Maturity	Capacity (MWh)	Power (MW)	Duration (Hours)	%Efficiency (Total cycles)	Total Cost ($/kW)	Cost $/kWh
Advanced Pb-acid	Demo	3.2-48	1-12	3.2-4	75-90 (4500)	2000-4600	625-1150
Na/s	Commercial	7.2	1	7.2	75 (4500)	3200-4000	445-555
Zn/Br flow	Demo	5-50	1-10	5	60-65 (>10,000)	1670-2015	340-1350
V redox	Demo	4-40	1-10	4	65-70 (>10,000)	3000-3310	750-830
Fe/Cr flow	R&D	4	1	4	75 (>10,000)	1200-1600	300-400
Zn/air	R&D	5.4	1	5.4	75 (4500)	1750-1900	325-350
Li-ion	Demo	4-24	1-10	2-4	90-94 (4500)	1800-4100	900-1700

Table 3 Characteristics of commercially available fuel cells for electric vehicles [Courtesy of EMC][72]

Parameter	Hydrogenics HyPM 65	Ballard MK 902 (LD)	eVionyx Zn-air FC
Fuel cell technology	PEM	PEM	Zinc-air
Peak operating efficiency (%)	55	50-60	70
Fuel	H_2 (99.99%)	H_2 (99.99%)	Zinc (solid)
Rated net power (kW) continuous	65	85	20
DC output voltage (V)	72	284	312
Specific power (W/Kg)	320*	885*	125-250
Power density (W/L)	306*	1133**	80-150
Durability (hours)	>6000	2116**	>2000
Start-stop cycles	±6000	N/A	N/A
Projection price (US $/kW)	N/A	73***	<100
Actual price (US $/kW)	>3000[2]	>3000[2]	<500

* Specific power and power density excluding hydrogen storage and auxiliary components

** Ballard 2005 achievement

*** Production volume of 500,000 units per year, excluding hydrogen storage

1.2.4 New Cathode Materials

The air cathode of Zn-air battery is one of the most expensive cell components and is largely responsible for limiting the performance of the cell. The most commonly employed catalyst for catalyzing the battery discharge is the platinum metal. The platinum is able to catalyze oxygen reduction reaction with high efficiency. Nevertheless, Pt is in limited reserve and has experienced increased price over the past decade (Fig. 7.) which have hindered the large-scale implementations for Zn-air battery technology. For instance, the air cathode of Alupower Ltd. has a price of $ $120m^{-2}$ and an energy cost of $ $50kW^{-1}$ at a high surface power density of $5kWm^{-2}$ with the cathode catalyst responsible for 50% of this cost[73]. As a result, the demand for cost-effective non-precious air cathode has increased the research and development of novel electrocatalysts.

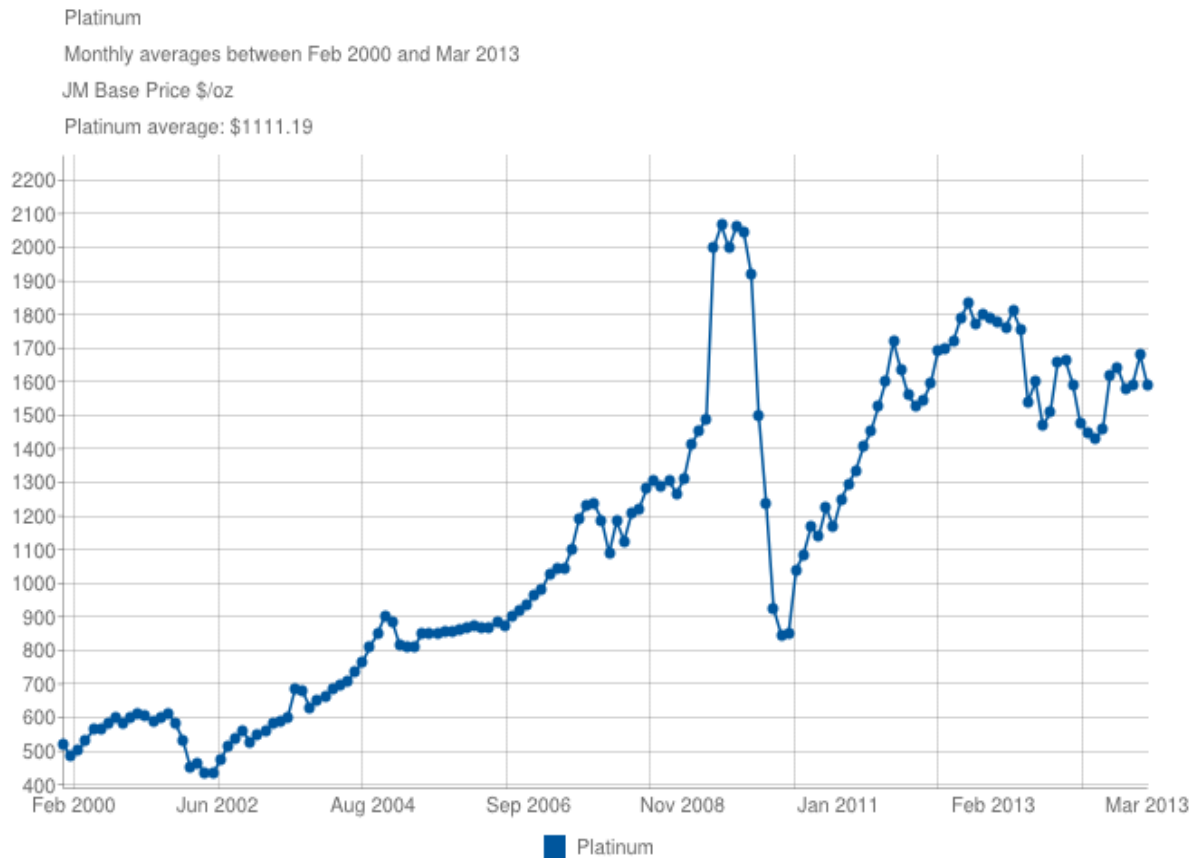

Fig.7. Price of Platinum metal between Feb, 2000 and Mar, 2013[74]

The current research on non-precious electrocatalysts focuses on three types of materials: carbonaceous materials, structured metal oxides and their hybrids as bifunctional catalysts. All these materials were studied by synthesizing their nanostructures with various morphologies. Carbon materials (e.g. carbon nanofibres, carbon nanotubes and graphene) are intensively studied as efficient ORR catalyst by introducing one or two ORR active species such as nitrogen[3], sulfur[4], boron[75] and phosphorous[6] into the carbon structure.Spinels and perovskites are potential candidates as low-cost electrocatalysts for both ORRs and OERs. Different shaped spinels such as nanocubes, nanoplatelets, and so forth has been synthesized with a variety of methods but they have not been quite used as electrocatalyst just by themselves.

Perovskites have been employed as the air cathode for solid oxide fuel cells due to the oxygen deficiency in their crystal structures. $LaNiO_3$ has been used as the electrocatalyst in metal-air batteries with moderate performance. Since spinels and perovskites are not very conductive and good catalytic activity requires fast electron transport, these metal oxides require attachment to a conducting surface. The hybrid bifunctional electrocatalyst adopted this idea by combing the metal-oxide and carbon surface. Liang et al[76] brought insights into the synergistic coupling between Co_3O_4 and graphene, and demonstrated excellent bifunctionality and stability of the hybrid material. This type of material has been the area of active pursuit.

1.3 Activated and Nitrogen-doped Carbon Nanofibres

Carbon nanofibres, as shown in Fig. 8., is recognized as one of the promising materials based on its nanostructure and particular properties, being expected in various applications such as catalysis for fuel cells and metal-air batteries. Nevertheless, CNF shows relatively low surface area from 50 to 350 m^2/g compared to activated carbons[77]. CNFs with high surface areas are expected to have improved performance, better ORR activity. Chemical activation with potassium hydroxide is a well-known method to activate carbon materials in order to achieve higher surface area[78]. Nevertheless, the activation mechanism is still under discussion[79-85]. In spite of a little information on the chemistry of alkaline activation, various examples have confirmed the increased surface area via KOH activation. Zhu et al.[86] reported using KOH chemical activation on exfoliated graphene to produce activated materials with an extremely high surface area ($3000 m^2 g^{-1}$). Although CNFs are possible to be activated for higher surface area, they generally exhibit poor inherent catalytic activity, particularly for ORRs in metal-air batteries. Nitrogen-doping is a commonly adopted methodology to introduce ORR active species into a

material. By coupling KOH activation with nitrogen-doping techniques on CNFs, their ORR activities are expected to be enhanced. Recently, Higgins et al[3] applied this method to fabricate activated, nitrogen-doped and exfoliated graphene for Li-air and Zn-air battery applications which obtained excellent cathode catalyst performance. CNFs are environmentally benign, low cost and commercially available materials. The fabrication methods of activated and nitrogen-doped carbon nanofibres from the commercial CNFs are straightforward and ideal for up-scalability to meet market demands. This process is able to optimize multiple aspects of CNF's properties that have the potential for utilization in high performance Zn-air battery technology.

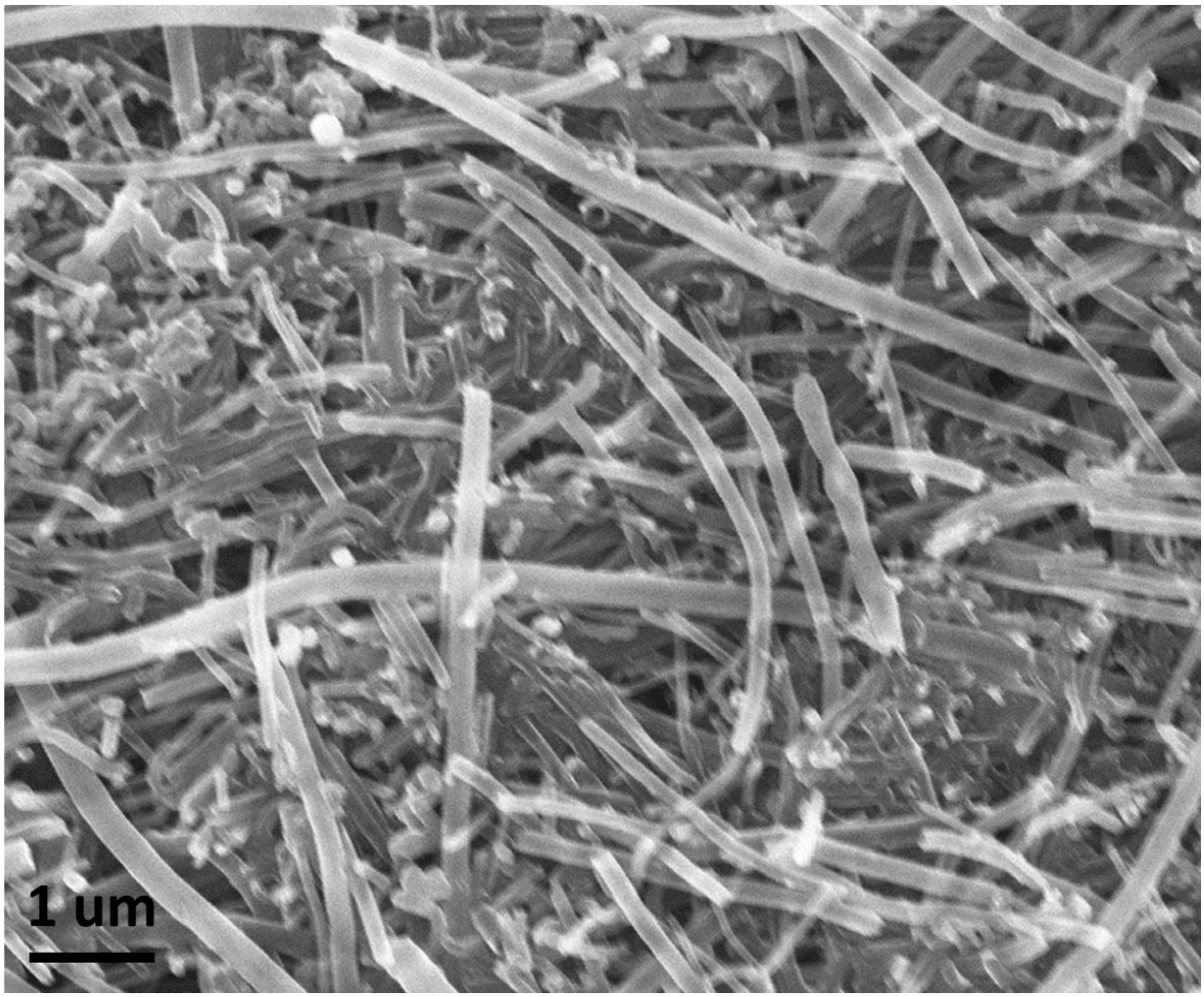

Fig.8. SEM image of Pristine CNF

1.4 Spinel Cobalt Oxide and Perovskite Lanthanum Nickelate

Nano-scaled materials with the size of 1-100nm have attracted considerable interest in recent years due to the departure of properties from the bulk phase. Over the past years, a variety of techniques have been applied to fabricate nanostructures of a broad class of materials with diverse morphologies. Through years of research, it is commonly understood that the behaviors of nanophase materials strongly depend on their shapes and sizes, which are thus a key factor of their performance and applications. In this regard, it is desirable to synthesize nanostructures with pre-designed morphologies and size distributions.

Spinel cobalt oxide stands as an important functional material because of its vast applications, especially in catalysis and energy storage. Spinel Co_3O_4, when falling in the nanosized regime, is expected to lead more attractive applications. Recently, Co_3O_4 and other spinels have been coupled with carbon materials such as graphene and carbon nanotubes as bifunctional catalysts[70, 76, 87, 88]. Nevertheless, none of these reported bifunctional catalysts demonstrated their morphology related bifunctional catalytic activities. In this work, Co_3O_4 nanocubes have been prepared via the synthesis method of Feng and coworkers[12]. A preliminary RDE evaluation was conducted on Co_3O_4 nanocubes. Moreover, Co_3O_4 nanocubes will be incorporated into hybrid materials via physically mixing with graphene and chemically attaching to carbon nanotubes.

Mixed electronic and ionic conductors such as ABO_3 perovskites (where A is a divalent metal ion and B is a tetrahedral metal) are promising cathode materials due to their high oxygen ion diffusivity and surface exchange properties[89]. Commonly adopted preparation methods for these kinds of materials are sol-gel methods such as Pechini method[90, 91]. Nevertheless, this methodology generally produces perovskites in large chunks which gave relatively low surface

area. A modified sol-gel method from Zhuang et al [92]was utilized in $LaNiO_3$ synthesis to obtain finer particle sizes and their ORR catalytic properties were explored.

This work serves as a preliminary study of spinels and perovskites for ORR/OER applications and builds a foundation for further research of hybrid bifunctional catalysts for Zn-air batteries.

1.5 Cubic Spinel Cobalt Oxide/Exfoliated and Nitrogen-doped Graphene

Among myriads of carbon materials, graphene is the most attractive to the scientific community due to various reasons. Graphene is a one atomic layer of graphite comprising sp^2 hybridized carbon atoms. Graphene has drawn a significant attention in recent years because of its extraordinary electrical conductivity (as high as 2200 S/m, depending on synthesis methods). graphene sheets offer high theoretical specific surface area as well as high mechanical strength and electronic conductivity[93]. Graphene can be prepared by various different methods such as chemical vapor deposition (CVD), mechanical exfoliation, oxidation and reduction of graphite, and liquid-phase exfoliation of graphite[94]. Amongst these methods, the synthetic route of the oxidation and reduction of graphite is widely used because a relatively large amount of graphene can be obtained. In practical situations, it is hard to obtain only a single layer of carbon, which is definition of graphene, during the synthesis. Normally, a few layers of aromatic carbons can be produced. For this reason, it is worth noting that the few layered byproduct can be called 'graphene' as well. Graphene has been employed as an electrocatalyst not only because the defect and edge sites presents active sites for electrocatalysis, but its unique morphology of porous structure helps accommodate the electrolyte and oxygen leading to effective catalytic

reactions. Moreover, doping heteroatoms such as boron, nitrogen or sulphur on graphene provides electrocatalytic active sites to improve the catalytic performances in an alkaline electrolyte. Not only graphene demonstrates catalytic activity towards ORR, but it is also used as a support material for precious metal catalysts or metal oxide catalysts to compensate for their low electrical conductivitiesby providing high surface area and electrical conductivity. Graphene can also be exfoliated to obtain higher surface area via fast thermal heating. As a result, graphene sheets are excellent candidates as conducting surfaces for metal oxides and can act as substrate to build hybrid material for energy applications. In this section, cubic spinel cobalt oxide was physically mixed with exfoliated and nitrogen-doped graphene sheets and the hybrid performance was evaluated with both RDE and Zn-air battery. The performance of the hybrid was compared to each of the hybrid component. The objective of this work demonstrates the potential application of cCo_3O_4/ExNG hybrid as cathode bifunctional catalyst in rechargeable Zn-air batteries and the feasibility of simplistic synthesis method.

1.6 Cubic Spinel Cobalt Oxide/Multi-walled Carbon Nanotubes

Metal oxide/ carbon hybrid materials as bifunctional catalytsts have triggered intensive research in recent years. To the best of my knowledge, the first metal oxide/carbon bifunctional catalysts for rechargeable Zn-air batteries was synthesized by a group of scientists from Paul Scherrer Institute, Switzerland[95]. In their experiments, calcium- and strontium-substituted rare earth cobaltate with perovskite structure was synthesized via a variety of methods. The perovkiste powders later acted as substrates for carbon nanotube growth by CVD method. Nevertheless, the catalytic activity of the hybrid material was not great. Using the same synthesis method but with lanthanum nickelate as substrate of nitrogen-doped carbon nanotubes by Chen et al.[35] afforded

a relatively high bifunctional catalytic activity. Starting in 2011, a series of research papers from Hongjie dai's group at the Stanford University brought more insights into this type of hybrid materials. Instead of employing CVD methods which destroys the crystal structure of the substrate, in-situ chemically attaching spinels to carbon surfaces such as graphene and carbon nanotubes provides an alternative synthesis process, which leaves the crystal structure of the metal oxide intact meanwhile affording excellent performance approaching Pt/C in alkaline condition[7, 76, 88]. Currently, more and more researchers are involved in synthesizing metal oxide/carbon hybrid materials. Nevertheless, the metal oxide morphology related bifunctional catalytic activity has never been reported. In this work, a facile hydrothermal route has been adopted to fabricate cubic spinel cobalt oxide/multi-walled carbon nanotube hybrid using acid-functionalized carbon nanotubes as structure directing/oxidizing agents. To the best of my knowledge, this is the first reported cubic Co_3O_4 and MWCNT hybrid material (cCo_3O_4/MWCNT) with outstanding bifunctionality and stability.

CHAPTER 2: Experimental

2.1 Cathode Catalysts Preparation Procedures

In this work, four different cathode catalysts were prepared:

- Activated and Nitrogen-doped Carbon Nanofibres
- Spinel Cobalt Oxide and Perovskite Lanthanum Nickelate
- Cubic Spinel Cobalt Oxide/Exfoliated and Nitrogen-doped Graphene
- Cubic Spinel Cobalt Oxide/Multi-walled Carbon Nanotubes

2.1.1 Activated and Nitrogen-doped Carbon Nanofibres

CNF (Sigma Aldrich, Product Number 719811) was soaked in 0.7M KOH and sonicated for 1 day to get a good dispersion. After sonication, the suspension was kept still for another day to achieve better KOH impregnation. The suspension was then vacuum filtered and the black product was collected and dried in oven at 60˚C overnight. To activate the KOH impregnated CNF, the sample was pyrolyzed at various temperature with a ramping rate of 5˚C/min to that temperature and dwelling for 1 hour with Ar flow at 100sccm. Once the pyrolysis is finished, the sample is collected and washed with copious amount of DDI until pH is neutral. For nitrogen-doping, the furnace was heated to 850˚C at 5˚C/min and dwell for 1 hour with Ar/NH_3 flow rate of 50sccm each. Preparation processes are shown in Fig. 9.

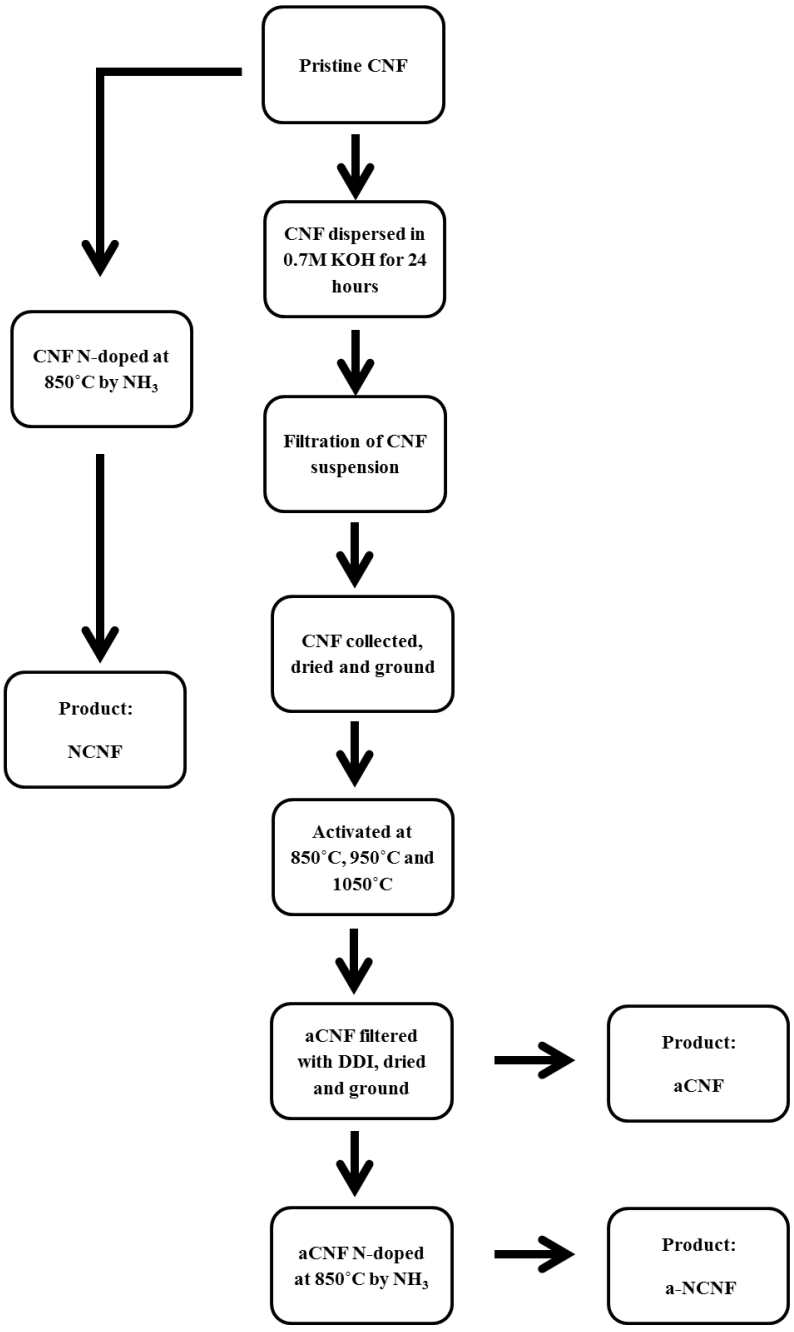

Fig.9. Flow chart of NCNF, aCNF and a-NCNF preparation processes

2.1.2 Spinel Cobalt Oxide and Perovskite Lanthanum Nickelate

Cubic spinel cobalt oxide: The cCo_3O_4 was prepared via the synthesis method of Feng et al[12]. Briefly, 1.2 g of NaOH (≥97.0%, Sigma-Aldrich) was dissolved in 100mL of ultrapure water in a three-necked round bottom flask followed by the addition of 90 g of $NaNO_3$ (Minimum 99.0%, Sigma-Aldrich). Air was continuously bubbled into the solution for the entire experiment. After half an hour, 20 ml of 1M $Co(NO_3) \cdot 6H_2O$ (≥98%, Sigma-Aldrich) was added to the solution. The oil bath was kept at 105˚C for 24 hours and the resulting black product was centrifuged with 2M HCl. The black product was further washed and collected for characterization. Preparation processes are shown in Fig. 10.

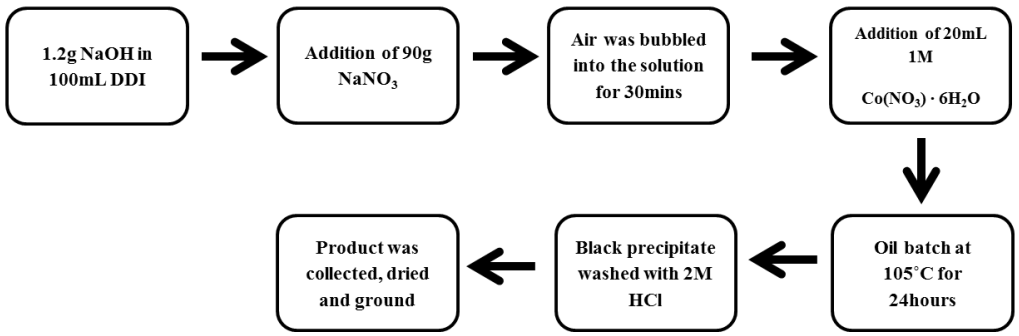

Fig.10. Flow chart of cubic spinel cobalt oxide preparation processes

Lanthanum nickelate: $La(NO_3)_3 \cdot 6H_2O$, $Ni(NO_3)_2 \cdot 6H_2O$ and citric acid were used as reagents. An aqueous solution of citric acid with a 10% excess over the number of ionic equivalents of cations was prepared. The aqueous solution of citric acid was added to various amount of Vulcan carbon, in which the mass ratios of Vulcan carbon to the theoretical mass of $LaNiO_3$ were 0:1, 1:1, 2:1 and 3:1, respectively. Then they were agitated vigorously for 4hours in room

temperature. Subsequently, the aqueous solutions of the stoichiometric metal nitrates were gradually added to the as-prepared solution and they were agitated for another 15min. The resulting solution was concentrated by slowly evaporating water until a gel was obtained. The gel was charred at 250˚C and kept for 12 hours to produce the solid amorphous citrate precursor. The precursor was milled and calcined in air at 650˚C for 4 hours. Preparation processes are shown in Fig. 11.

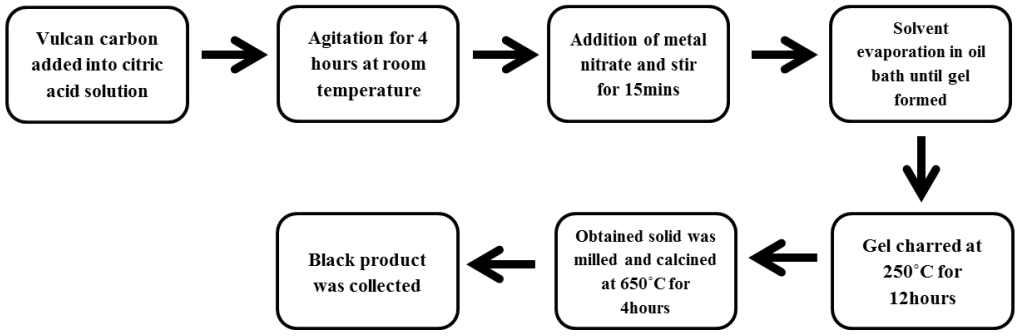

Fig.11. Flow chart of lanthanum nickelate preparation processes

2.1.3 Cubic Spinel Cobalt Oxide/Exfoliated and Nitrogen-doped Graphene

Graphite oxide (GO) was prepared via the method of Marcano et al[96]. Briefly, 40ml of phosphoric acid and 360ml of sulfuric acid was mixed in an ice bath. After fully mixed, 2g of graphite powder was added into the acid mixture followed by slowly addition of 18g of potassium permanganate. Once it became homogeneous, the solution was transferred into an oil bath at 55˚C with constant stirring for 16 hours. After the reaction completed, the solution was transferred into an ice bath for cooling and 400ml of DDI water was then added into the solution

dropwise followed by 40ml of hydrogen peroxide to wash off the manganese. The GO was further washed multiple times with DDI, ethanol and 30% of HCl and collected by freeze drying for synthesis of exfoliated and nitrogen-doped graphene (ExNG). ExNG was synthesized via thermal exfoliation of GO in ammonia gas. GO, loaded on a small quartz tube, was positioned into a long qurtz tube on a furnace with argon gas flowing at 50 sccm. Once the furnace was heated up to 900˚C, ammonia gas was allowed flowing at 50 sccm and the long tube was pushed into the furnace with the GO positioned at the center. After 10 mins, the GO had been fully exfoliated and nitrogen-doped into ExNG. The ExNG was collected for further characterization. cCo_3O_4 /ExNG was prepared by mixing cCo_3O_4 and ExNG with 1to1 ratio. Preparation processes are shown in Fig. 12.

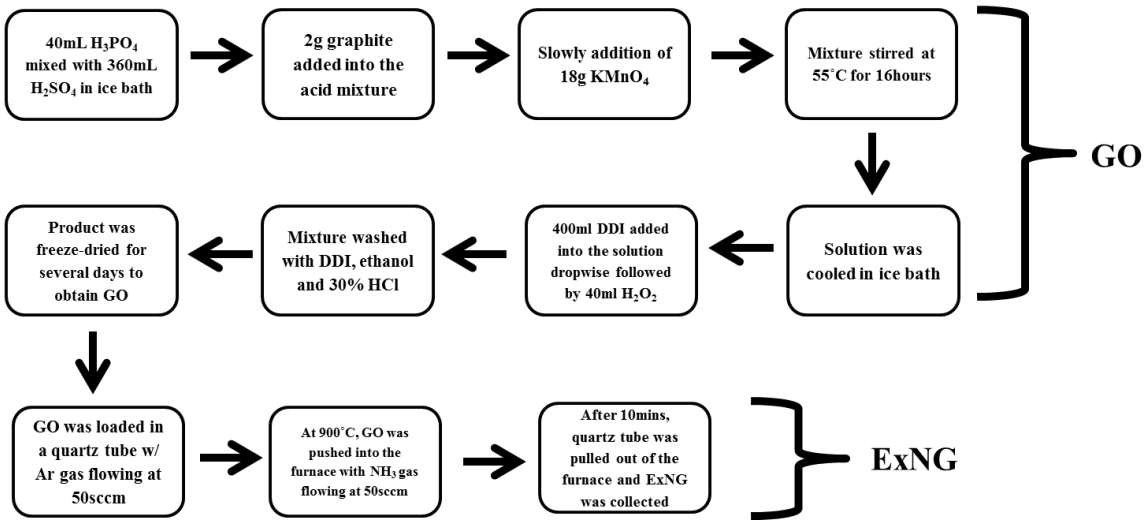

Fig.12. Flow chart of exfoliated and nitrogen-doped graphene preparation processes

2.1.4 Cubic Spinel Cobalt Oxide/Multi-walled Carbon Nanotubes

The cCo_3O_4 was prepared via the synthesis method of Feng et al[12]. The cCo_3O_4/MWCNT was prepared through a hydrothermal method with acid-functionalized multi-walled carbon nanotube (MWCNT) and $Co(CH_3COO)_2 \cdot 4H_2O$ (Reagent grade, Sigma-Aldrich) as starting materials. MWCNTs were purchased from MER Corporation., USA. The MWCNTs were treated in 6M nitric acid at 110˚C for 5 hours followed by washing with copious amount water and dried in the oven for further uses. Typically, 45 mg of $Co(CH_3COO)_2 \cdot 4H_2O$ was dissolved in 10 mL of ultrapure water, into which ammonia was added to adjust the pH of solution to 8. Afterwards, 15 mg of the acid-treated MWCNT was dispersed in the above solution by stirring and followed by ultrasonication. The solution was then transferred into an autoclave for 5 hours reaction at 150 ˚C. The resulting black product was collected by centrifuge and dried overnight. Preparation processes are shown in Fig. 13.

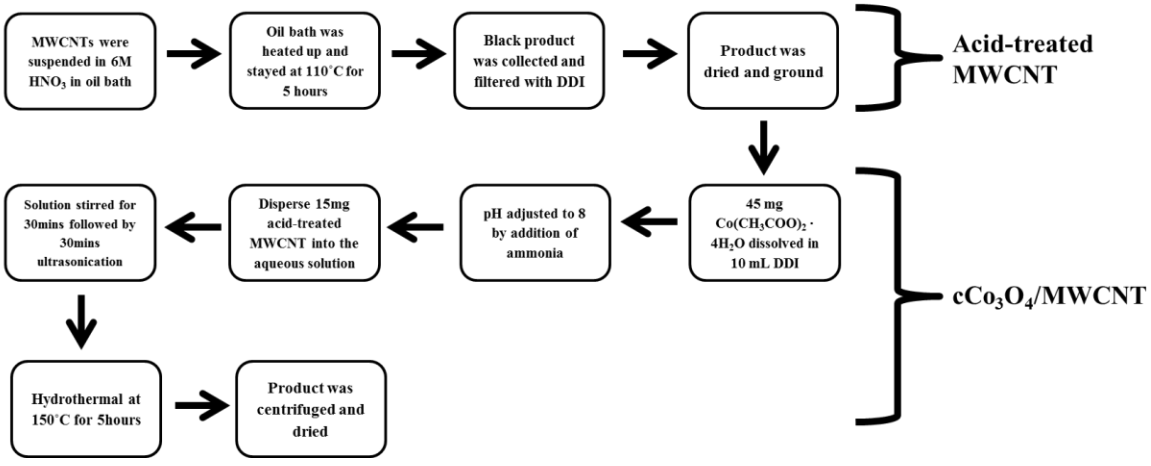

Fig.13. Flow chart of cubic spinel cobalt oxide/multi-walled carbon nanotubes hybrid preparation processes

2.2 Material Characterization Techniques

Several material characterization techniques were adopted in the work to analyze synthesized samples physically and electrochemically. Physical characterizations can assist to establish fundamental understandings of the surface compositions, specific structures and morphologies of the substance which is especially crucial to nanostructured materials. Moreover, for the purposes of ORR/OER catalytic activities investigations, the electrochemical characterizations must be effectively coupled with detailed physical characterization techniques. In this section, characterization techniques utilized throughout this work were introduced with their applications and working mechanisms.

2.2.1 Elemental and morphological analysis

2.2.1.1 Scanning electron microscopy (SEM)

Scanning electron microscopy is a powerful and versatile tool to investigate the surface morphology of materials in the range from several nanometers to micrometer scale. Conventional light miscroscopes use a series of glass lenses to bend light waves and create a magnified image. The scanning electron microscope creates the magnified images by using electrons instead of light waves. An electron gun emits a beam of high energy electrons and this beam travels downward through a series of magnetic lenses designed to focus the electrons to a very fine spot. As the electron beam hits each spot on the sample, secondary electrons are knocked loose from its surface. A detector courts these electrons and sends the signal to an amplifier. The final image is built up from the number of electrons emitted from each spot on the sample. Scanning electron microscopy is employed in this work to verify the successful synthesis of the desired morphologies.

2.2.1.2 Transmission electron microscopy (TEM)

The transmission electron microscope is ideal for a number of different fields, especially for nanostructured materials characterizations. The transmission electron microscope uses a high energy electron beam transmitted through a very thin sample to image and analyze the nanostructure of materials with atomic scale resolution. The electrons are focused with electromagnetic lenses and images are observed on a fluorescent screen. The transmission electron microscopy offers a more powerful magnification than the scanning electron microscopy with high-quality and detailed images.

2.2.1.3 X-ray diffraction (XRD)

X-ray diffraction technique is a key characterization technique to determine the crystal structures of materials. X-rays are employed to generate the diffraction pattern of the crystal because wavelength of X-ray is typically the same order of magnitude (1–100 angstroms) as the spacing between atomic planes in the crystal. The principle of X-ray diffraction obeysthewell-known Bragg's law which is shown in the following equation

$$2d\ sin\ \theta\ =\ n\lambda$$

where n, λ, d, and θ represent the order of the spectrum (any integer), the wavelength of the X-rays, the spacing between diffracting planes, and the incident angle, respectively. As a result, X-ray diffraction patterns, which is the intensity of diffracted X-ray versus the angle, are obtained. The patterns having the intensity maxima and the angles are compared with a database containing the theoretical diffraction patterns of crystal structures to identify the sample's crystal

phase. It is worth noting that XRD cannot provide the patterns of amorphous materials because they are in random orientations yielding diffuse patterns.

2.2.1.4 X-ray photoelectron microscopy (XPS)

X-ray photoelectron spectroscopy, also known as electron spectroscopy for chemical analysis, is a prevalent characterization tool for the investigation of elemental composition, empirical formula, chemical state and electronic states of an element. In principle, x-rays with known energy irradiate on analyte, causing emission of electrons by photoelectric effect and the kinetic energy and number of electrons that escape from the material's surface (top 1 to 10 nm) are detected and analyzed based on the electron binding energy. The binding energy spectrum versus the number of electrons can directly identify the elements on the surface of the material and provide the relative amounts of each element. In this project, XPS is utilized to confirm and quantify nitrogen doping on carbon nanofibres and graphene by detecting nitrogen content and its binding configurations on the structure.

2.2.1.5 Thermogravimetric analysis (TGA)

TGA was utilized to study the weight change of a substance responded to the elevation of temperature. In this thesis, TGA was adopted to analyze the composition of spinel cobalt oxide/multi-walled carbon nanotubes hybrid. The TGA experiment is performed by heating the sample of known mass in a platinum pan either in pure N_2 or N_2/air (50/50 mixture by volume) environment. The temperature set point, ramp rate and dwell time can be controlled by the

coupled software. In the situation of cubic spinel cobalt oxide/multi-walled carbon nanotubes hybrid, the hybrid was heated up to 800C in N_2/air environment at a ramp rate of 5˚C/min

2.2.2 Electrochemical analysis

2.2.2.1 Rotating disc electrode testing (RDE)

A RDE measurement is an electrochemical technique widely used to study the mechanism of redox reactions and screen materials based on the electrochemical activities. A RDE is simply defined as a hydrodynamic working electrode in an electrochemical cell. The RDE consists of a disk electrode imbedded in a rotating rod of an insulating material and rotating of the disk electrode creates a totally defined solution flow pattern in which the mass transport of the species is almost complete by convection. In the proposed projects, Glassy carbon disk electrodes coated with the catalyst material suspension made by mixing with 0.5 wt% Nafion in ethanol is used as a working electrode, saturated calomel electrode (SCE) is used as a reference electrode and Pt wire is used as a counter electrode. The basic setup of RDE system along with a cross-section image of the glassy carbon electrode adopted throughout this work is shown in Fig. 14. and Fig. 15, respectively. Mostly RDE is utilized in combination with linear sweep voltammetry (LSV) technique in which potential range for redox reactions is swept and the current produced is detected while the electrode is rotated at various speeds. The results from the RDE measurements at different rotating rates can be used to study the reaction kinetics of ORR in 0.1 M KOH, which is employ in the project, via the Koutecky-Levich (K-L) equation as follows

$$\frac{1}{i} = \frac{1}{i_k} + \frac{1}{i_d} \qquad (6)$$

$$i_k = nFkC_o \qquad (7)$$

$$i_d = 0.62nFD_o^{2/3}\upsilon^{-1/6}C_o\omega^{1/2} \qquad (8)$$

In the above equation, i_k and i_d is the kinetic current and limiting current density, respectively, F is the Faraday constant (96 485 C mol^{-1}), k is the rate constant for ORR (m s-1), D_o is the diffusion coefficient of O_2 (1.9 x 10-5 cm^2 s^{-1}) in 0.1 M KOH, υ is the kinematic viscosity of 0.1 M KOH (0.01 cm^2 s^{-1}), C_o is the concentration of O_2 in the electrolyte (1.1 x 10^{-6} mol cm^{-3}) and ω is the angular frequency of the rotation (rad s^{-1})and . By linear fitting the Koutecky-Levich plots of i^{-1} vs $\omega^{-0.5}$ one can obtain the electron number (n) and rate constant (k) for ORR. Cyclic voltammetry (CV) for OERs was characterized within the range of 0 to 1V with 900 rpm rotation speed in N_2 saturated 0.1M KOH for 500 cycles. After cycling, linear sweep voltammetry were measured again in the same way as previously stated. The initial and final performance obtained before and after the CV cycling were compared in order to evaluate the durability of a catalyst.

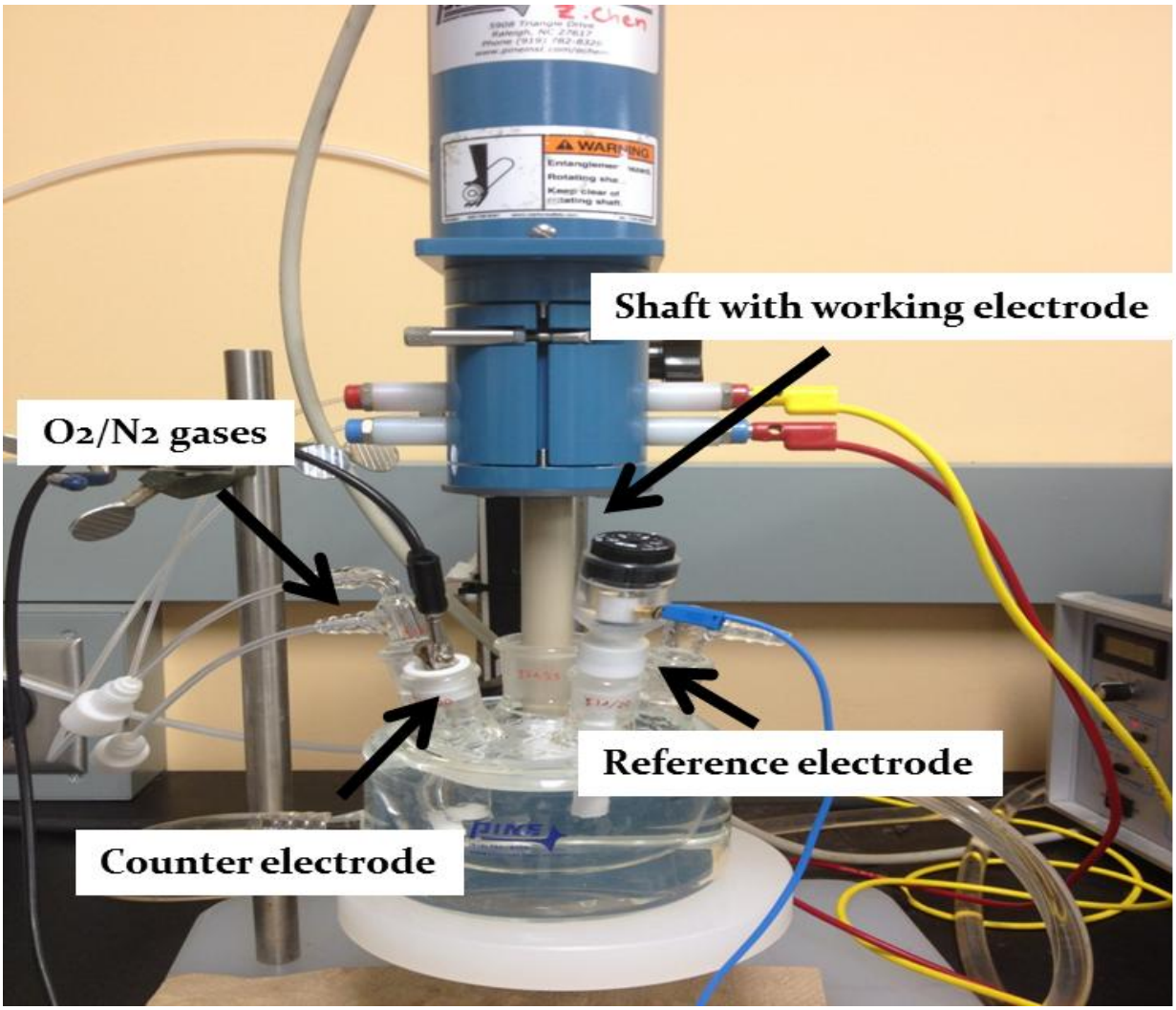

Fig.14. Setup of the RDE system with major components labeled.

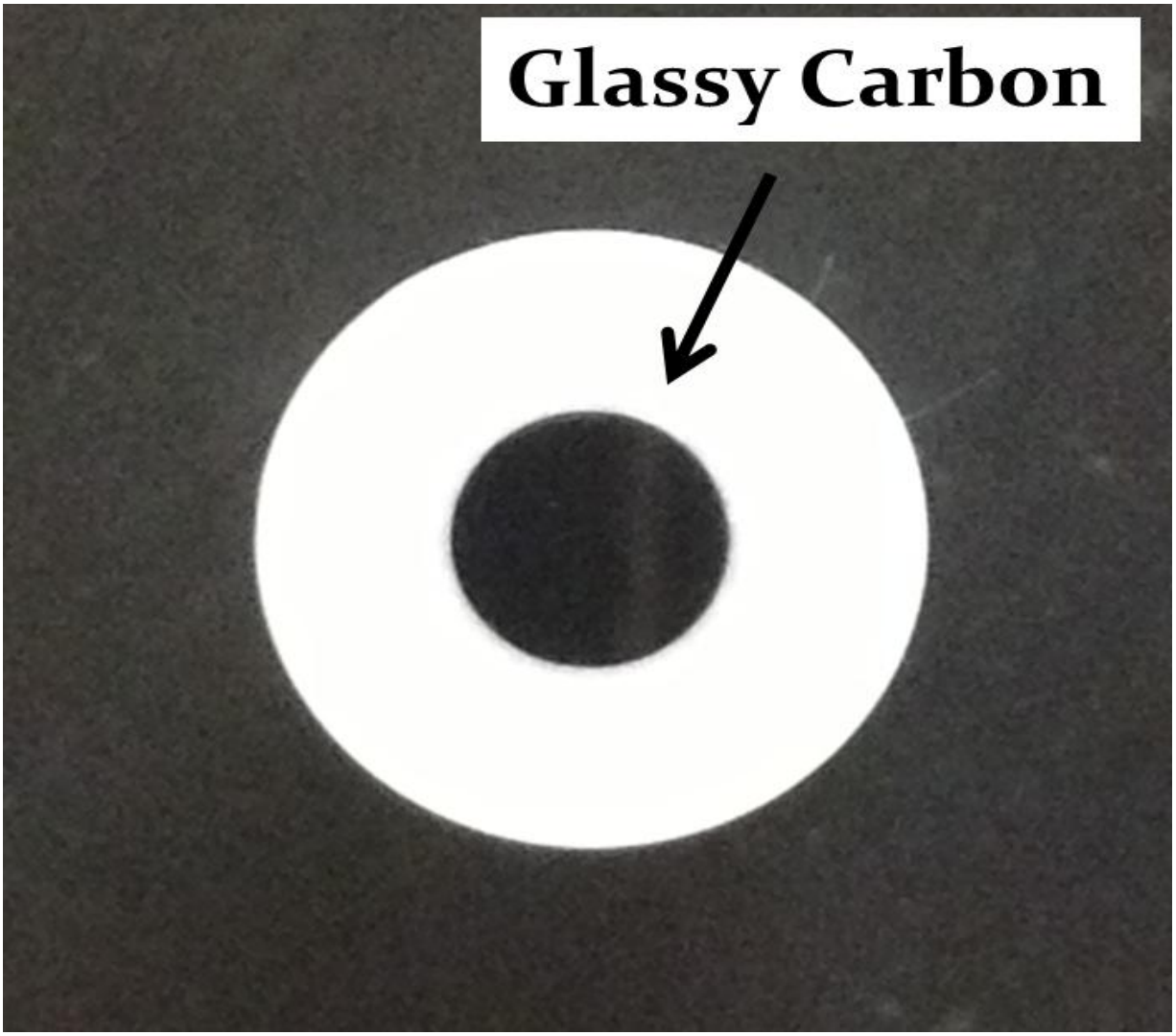

Fig.15. Cross-section image of the glassy carbon electrode

2.2.2.2 Electrocatalyst evaluations in Zn-air batteries

Zn-air battery testings of the electrocatalysts were performed using a multichannel potentiostat (Princeton Applied Research, VersaSTAT MC) with home-made Zn-air batteriesshown in Fig. 16. A polished zinc plate and a piece of catalyst-coated gas diffusion layer (Ion Power Inc., SGL Carbon 10 BB, 2.5 cm by 2.5 cm) were used at the anode and cathode, respectively. Microporous membrane (25 μm polypropylene membrane, Celgard 5550) was used as a separator and

stainless steel mesh was used as current collectors. The electrolyte used in the Zn-air battery was 6 M KOH for the highest ionic conductivity.

Based on the battery design, the effective area of the gas diffusion layer being exposed to the electrolyte is 2.84 cm^2. The procedures for coating the electrocatalyst onto the gas diffusion layer are the following. First of all, 9.4 mg of catalyst was dispersed in 1 mL of isopropanol and sonicated for 30 minutes. Following this, 67 μL of 5 wt. % Nafion solution was added and the mixture was sonicated for 30 minutes to form the catalyst ink. The catalyst ink was sprayed onto the gas diffusion layer with a conventional airbrush. After spraying, the gas diffusion electrode is dried at 80 °C for 1 h. The catalyst loading is determined by the difference in the weight of the gas diffusion layer before and after spraying. All the catalysts studied in this work were coated onto the gas diffusion layer using an airbrush to achieve a loading of ca. 1.5 $mgcm^{-2}$. The Zn-air cell used for the catalysts evaluations is shown in Fig. 17 along with its components and assembling sequence.

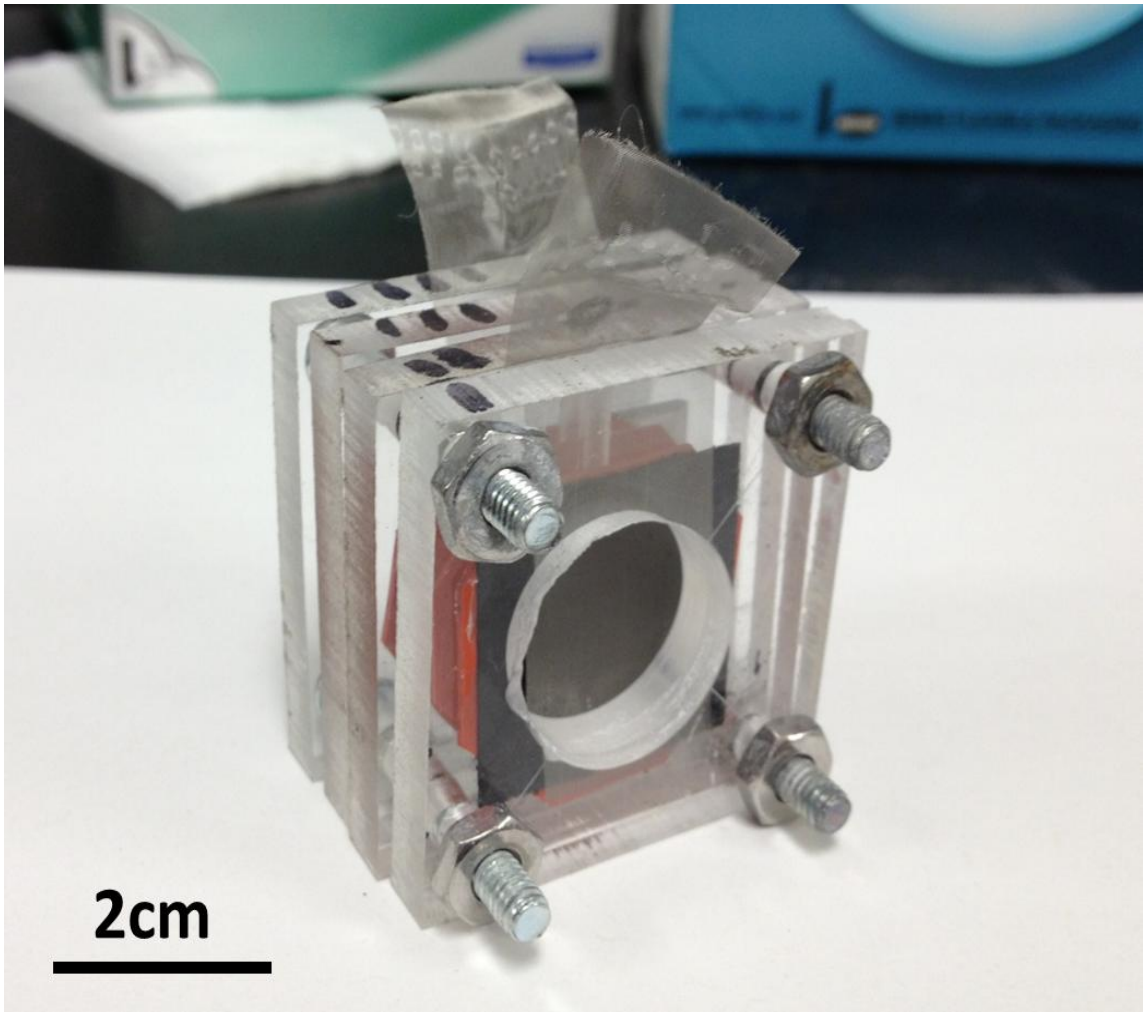

Fig.16. The Zn-air cell used for catalyst evaluations

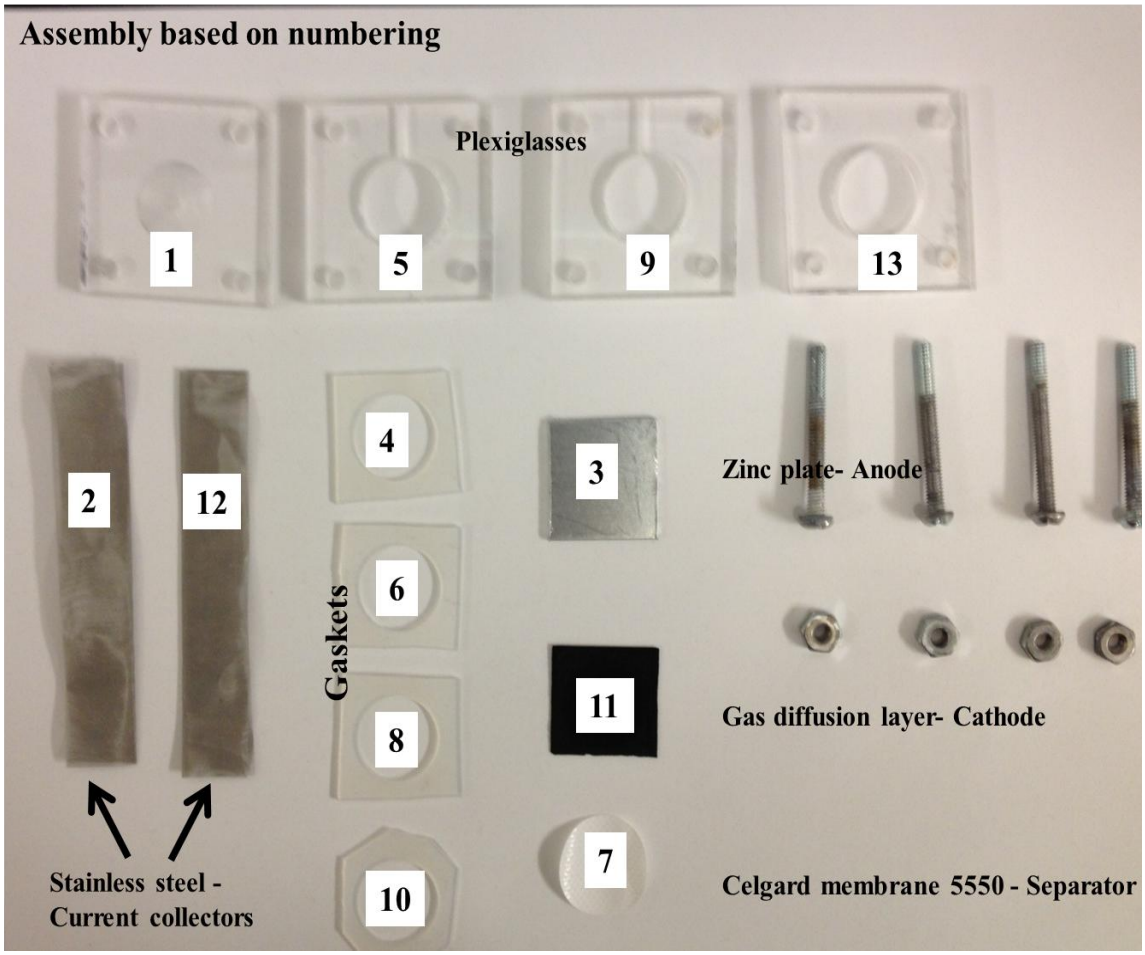

Fig.17. Zn-air cell components along with the assembling sequence.

A galvanodynamic method was used to discharge and charge the battery to 200 mA. The potential difference between the cathode and the anode was determined to be the open circuit voltage. Electrochemical impedance spectroscopy was performed from 100 kHz to 0.1 Hz with AC amplitude of 20 mV. The electrochemical impedance spectroscopy data was fitted with selected equivalent circuit (Fig. 18) using Zsimpwin software. Five elements are shown in the equivalent circuit, R_s, Q_{int}, R_{int}, Q_{dl} and R_{ct}. Similar equivalent circuit has been proposed by various researchers to investigate the electrode processes of the air electrode for zinc air battery[97, 98]. The R_s component of the equivalent circuit represents the resistance associated

with various battery components, such as the electrolyte and contact resistances. The solid to electrolyte interface resistance can be present in the battery and is illustrated by R_{int}. R_{ct} represents the charge transfer resistance encountered during electrochemical reactions on the electrode. The constant phase elements, Q_{int} and Q_{dl} are included in the equivalent circuit for modeling the non-faradaic processes. The constant phase elements are used in place of the conventional capacitance due to the use of porous electrodes as well as the non-homogeneity in the system. The Q_{int} refers to the capacitance arises from the solid electrolyte interface on the air electrode, and Q_{dl} represents the double layer capacitance. With the equivalent circuit, the values of different electrochemical elements can be determined.

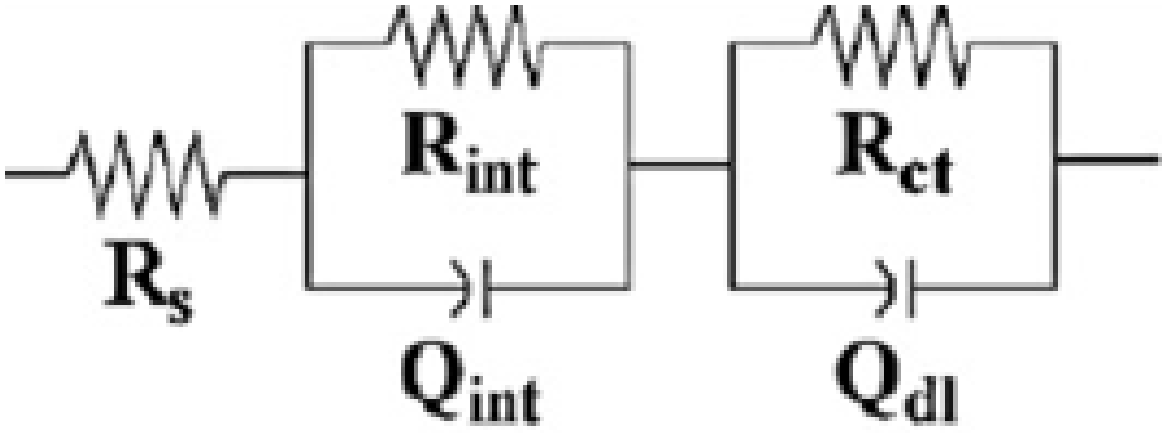

Fig.18 Equivalent circuit employed to model the electrochemical impedance data[3, 35, 99]

CHAPTER 3: Results and Discussion

3.1 Introduction to Studied Catalysts

Carbon materials for ORR applications have been actively studied for the past few years. Introducing ORR active species to the carbon structure has been an effective way to produce low cost electrocatalysts. Nitrogen doped carbon nanotubes and graphene are two of the most well-known non-precious ORR catalysts and have been studied over years in the scientific community. Nevertheless, carbon nanofibre, another important carbon material, has not been raised with much attention as a candidate for ORR catalysis. Carbon nanofibres are commercially available with much lower price than carbon nanotubes and graphene which is critical for its potential as ORR catalyst. By increasing surface area of CNFs and introducing nitrogen species to its structure via simple methods, CNF could potentially replace the state of the art Pt/C catalyst.

An excellent bifunctional catalyst allows Zn-air batteries to be electrically recharged and discharged with many cycles. Traditional noble metal alloy bifunctional catalyst is highly efficient but price limits its large-scale applications. Hongjie dai's group from Stanford University has brought insight into coupling spinel metal oxides with graphene as high performance and durable non-precious bifunctional catalysts[88, 100]. Spinels and perovskites have been studied for various applications, but as electrocatalyst, the conductivities of these metal oxides need to be enhanced because of the required fast electron transfer. Several research papers from Hongjie dai's group have shown the synergistic effect between the metal oxide and the carbon material. However, it is well believed that the electrochemical activities of nanostructured catalysts are closely related to their morphologies. But the morphology related bifunctional catalytic activities have never been reported, thus the in-situ synthesized

cCo_3O_4/MWCNT hybrid is worth studying and the studies of Co_3O_4 and $LaNiO_3$ laid a strong foundation towards this objective. In this study, four different types of catalysts have been explored and the experiemental results are presented below. The four different types of catalysts are:

- Activated and Nitrogen-doped Carbon Nanofibres
- Spinel Cobalt Oxide and Perovskite Lanthanum Nickelate
- Cubic Spinel Cobalt Oxide/Exfoliated and Nitrogen-doped Graphene
- Cubic Spinel Cobalt Oxide/Multi-walled Carbon Nanotubes

The properties of activated and nitrogen-doped carbon nanofibres, spinel cobalt oxide and perovskite lanthanum nickelate were studied at the beginning of this work mainly because the synthesis of metal oxide/carbon hybrid materials required detailed understandings of their individual components. A deep understanding of the synthesis process, catalytic activities and morphologies of metal oxides and carbon material will help the evaluations and discussions towards hybrid materials which consist of them.

3.2 Activated and Nitrogen-doped Carbon Nanofibres

3.2.1 Results and Discussion

Various activation temperatures (850˚C, 950˚C, 1050˚C) were selected to explore the effect of activation temperature on CNFs nitrogen-doped at the same condition towards the ORR activity shown in Fig. 19. The RDE linear sweep voltammetry measured at 900rpm indicated that the highest ORR activity was achieved for activation at 950˚C. By activation and nitrogen-doping,

a(950)-NCNF showed enhanced ORR half-wave potential, 26% greater than pristine CNFs and limiting current density increase of 17% compared to the pristine CNFs. The activation temperature was optimized at 950˚C and is used to investigate the effect of nitrogen-doping on activated CNFs in the following study.

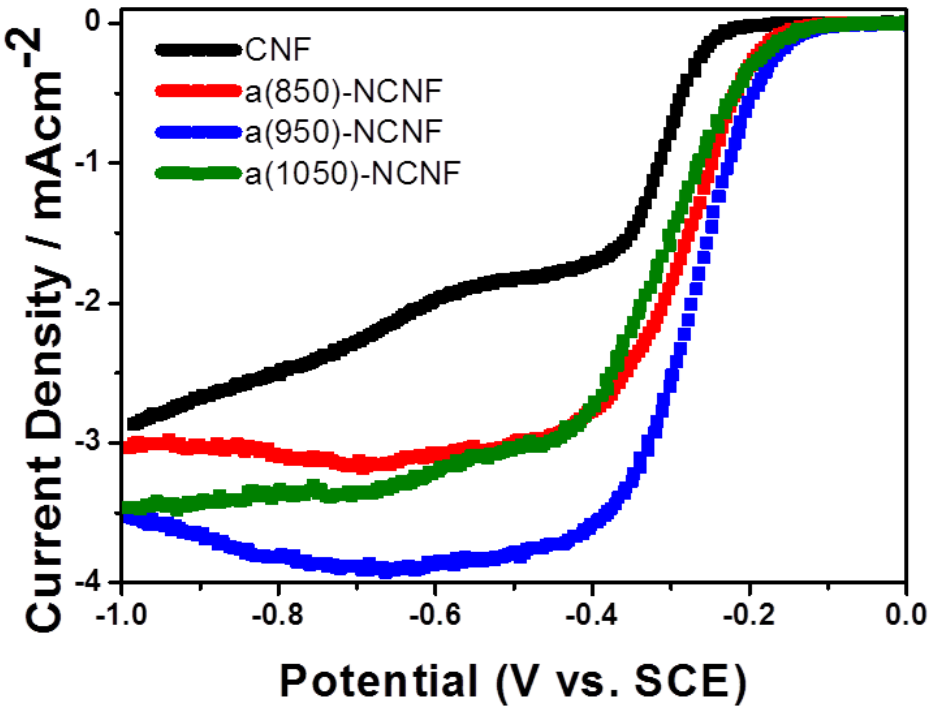

Fig.19. ORR comparisons among nitrogen-doped CNFs activated at different temperatures, 850˚C, 950˚C and 1050˚C

To further realize the effects of activation and nitrogen-doping on the CNFs, the ORR activities of CNF, NCNF, a(950)-CNF and a(950)-NCNF were measured and compared in Fig.20(a). The linear sweep voltammetry clearly indicated a trend of ORR performance changes after one treatment or both. Activated and nitrogen-doped CNF demonstrated the best ORR activity. A more intuitive comparison of the selected CNFs was shown by the OH^- selectivity in Fig. 20(b).

The a(950)-NCNF has the highest OH^- selectivity (above 95%) in the given range of potential which indicated it is more preferred to catalyze the 4 electron transfer pathway of ORR.

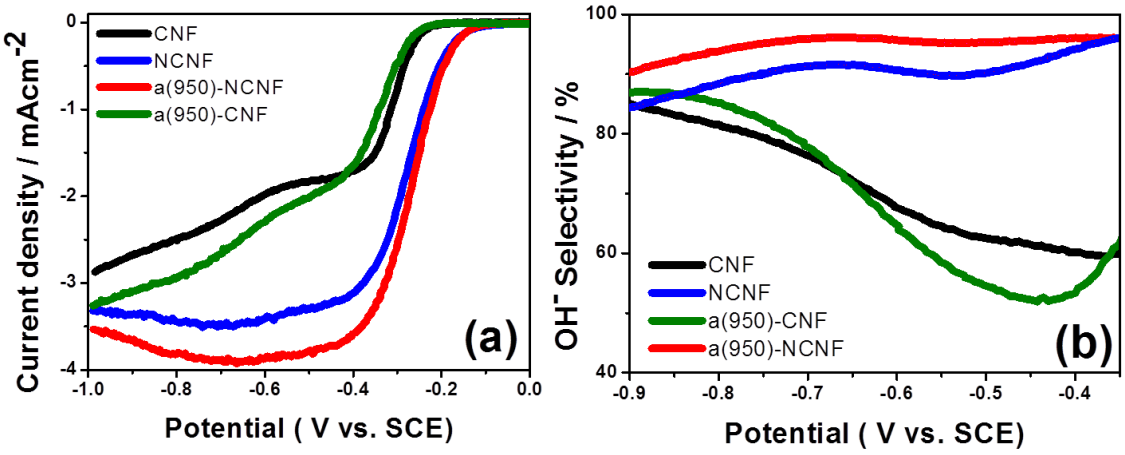

Fig.20. The effects of activation and nitrogen-doping on CNFs (a); The OH- selectivity of studied CNFs (b)

In order to further investigate the origin of the improved ORR activities, XPS was utilized on those CNFs activated at various temperature but nitrogen-doped at the same condition. The surface elemental spectrum of the selected CNFs was shown in Fig.21(a) and the elemental compositions of those CNFs calculated from the XPS data were tabulated in Table 4. High resolution N 1s spectrum shown in Fig. 21(b) indicates the presence of 4 types of nitrogen species. The amount of nitrogen content proportionally related to their ORR performance in RDE with a(950)-NCNF being the highest of four. Increasing the ORR active nitrogen species leads to the increase in ORR activity. The high resolution XPS showed the similar nitrogen dopant configuration. Combing the RDE data from Fig.19 and Table 4, it is assumed that there is a possible trade-off activated CNF surface area and oxygenated species.

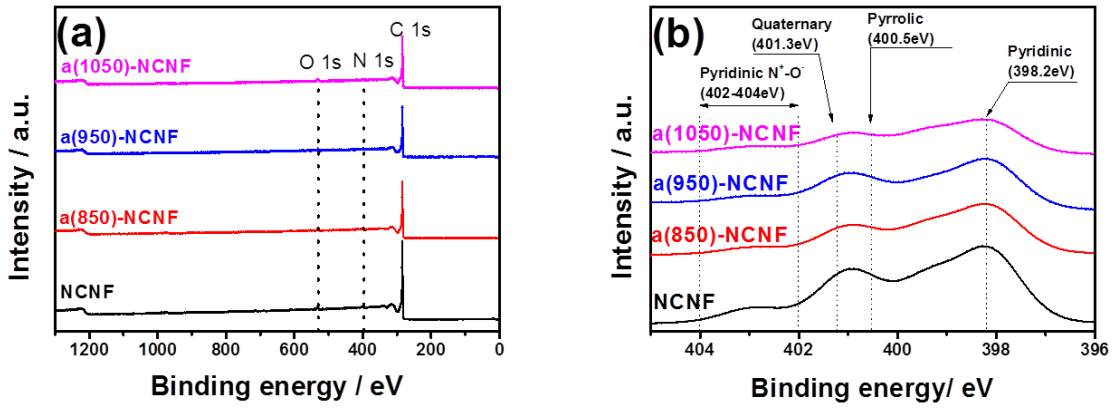

Fig.21. XPS spectra of NCNF, a(850)-NCNF, a(950)-NCNF and a(1050)-NCNF (a); High resolution N 1S signals of NCNF, a(850)-NCNF, a(950)-NCNF and a(1050)-NCNF with different nitrogen species labeled (b)

Table 4 Elemental compositions of NCNF, a(850)-NCNF, a(950)-NCNF and a(1050)-NCNF

Composition (at. %)	NCNF	a(850)-NCNF	a(950)-NCNF	a(1050)-NCNF
Carbon	95.62	95.41	95.78	96.33
Nitrogen	2.21	2.03	2.26	1.74
Oxygen	2.16	2.56	1.96	1.93

Based on the promising RDE performance, activated and nitrogen-doped CNFs were evaluated in metal-air battery adopting the zinc plate anode in a realistic condition. The discharge curves of Zn-air cells adopting various CNFs at the cathode were assembled and evaluated along with the state of the art catalyst Pt/C shown in Fig. 22(a). Among all the catalysts tested, Pt/C showed the highest voltage at 70mAcm^{-2} current density followed by a(950)-NCNF and pristine CNF showed the lowest voltage at the same current density tabulated in Table 5. The discharge data

obtained from Zn-air cell evaluations correspond to the ORR performance from the RDE evaluations.Electrochemical impedance spectroscopy (EIS) was adopted to further confirm the excellent ORR activities of activated and nitrogen-doped CNF. The charge-transfer resistance obtained from EIS is an indicator of the ORR activity and corresponds to the larger semi-circle on the Nyquist plot of Fig.22(b). In Table 6, Pt/C demonstrated the lowest charge-transfer resistance (Rct) and a(950)-NCNFbeing the lowest one among all the CNFs. After KOH activation and nitrogen-doping, the charge transfer resistance of pristine CNFs decreased by ~46% which clearly indicated an enhancement of ORR catalytic activity.

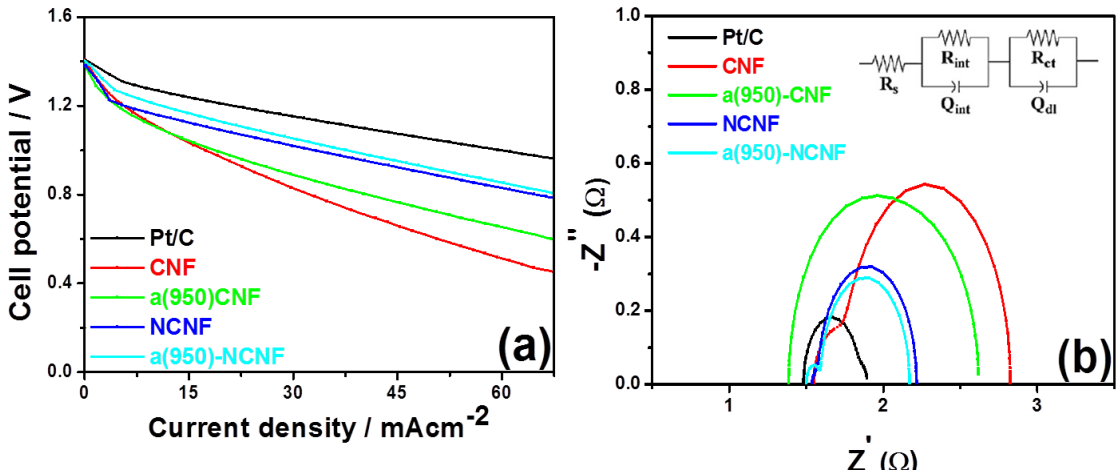

Fig.22. Discharge curves of Pt/C, CNF, a(950)-CNF, NCNF, a(950)-NCNF evaluated in Zn-air cells (a); Nyquist plots of Pt/C, CNF, a(950)-CNF, NCNF, a(950)-NCNF with the equivalent circuit inset (b)

Table 5 The cell voltage comparisons of Pt/C, CNF, a(950)-CNF, NCNF, a(950)-NCNF at 70mA/cm2

Catalyst	Cell potential @ 70mAcm^2 (V)
CNF	0.44
a(950)-CNF	0.59
a(950)-NCNF	0.80
NCNF	0.77
Pt/C	0.95

Table 6 Equivalent circuit elements and their respective values (Ω) for the air electrode

	R_s	R_{int}	R_{ct}	Q_{int}	Q_{dl}
CNF	1.6	0.203	1.07	6.02E-6	0.00308
a(950)-CNF	1.4	0.509	0.722	0.120	2.31E-4
a(950)-NCNF	1.5	10.1	0.580	0.000639	0.0157
NCNF	1.5	0.386	0.639	0.00620	0.639
Pt/C	1.44	0.0581	0.357	0.650	0.0677

3.2.2 Summary and Conclusion

High ORR active nitrogen-doped CNF material was fabricated by KOH activation coupled with nitrogen-doping with NH_3 which is a simplistic, readily up-scalable manufacturing process. Their high performance was evaluated through electrochemical characterizations and further confirmed by zinc air cells applications and electrochemical impedance spectroscopy. This work explored the possibility of producing low cost, easy-to-fabricate, high performance ORR catalyst for metal-air battery applications.

3.3 Spinel Cobalt Oxide and Perovskite Lanthanum Nickelate

3.3.1 Results and Discussion

Successful synthesis of Co_3O_4 nanocubes through in-situ method has been confirmed by both TEM image and XRD pattern, shown in Fig. 23(a) and 23(b), respectively. TEM image indicated the size of synthesized nanocube is ~45nm. The XRD patterns with crystal plane labeled demonstrated the successful synthesis of desired spinel structure.

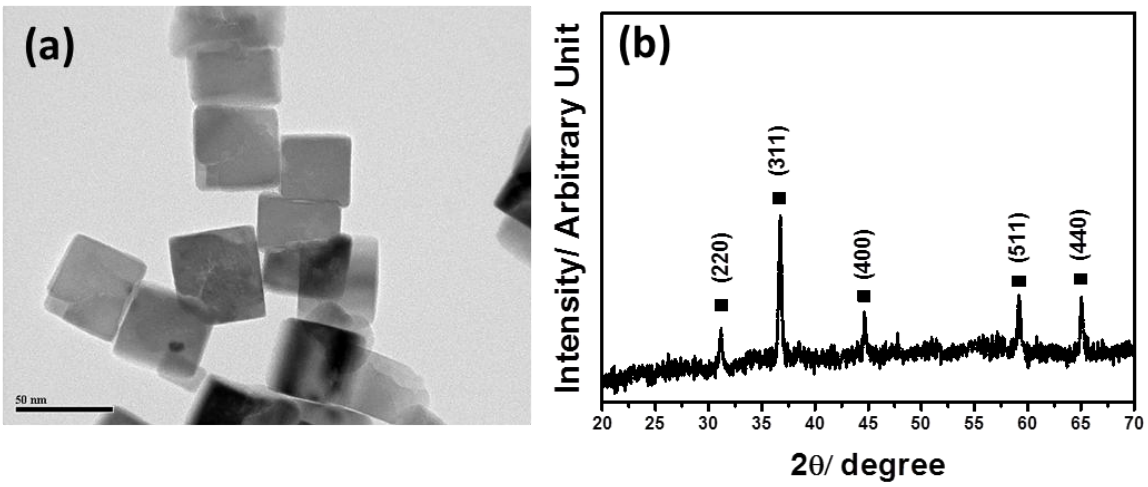

Fig.23. TEM image of the synthesized cubic spinel cobalt oxide (a); XRD pattern of the cubic cobalt oxide with crystal planes labeled (b)

The ORR and OER catalytic activities of cCo_3O_4were evaluated through RDE before and aftercyclic voltammetry cycling. As can be seen in Fig. 24(a) and Fig. 24(b), Co_3O_4 nanocubes exhibited moderate ORR and OER performance before cyclic voltammetry cycling, however after 500 cycles of cyclic voltammetry cycling from 0 to 1V, the ORR and OER performance dropped significantly. The ORR onset potential decreased by 50% and the OER limiting current at 1V decreased from ca. $15mAcm^{-2}$ to almost zero current density. The low intrinsic conductivity of the cobalt oxide limits its initial ORR and OER activities. Attaching cobalt oxide to a conducting surface such as a carbon surface would expect to improve its initial ORR and OER performance and possibly durability

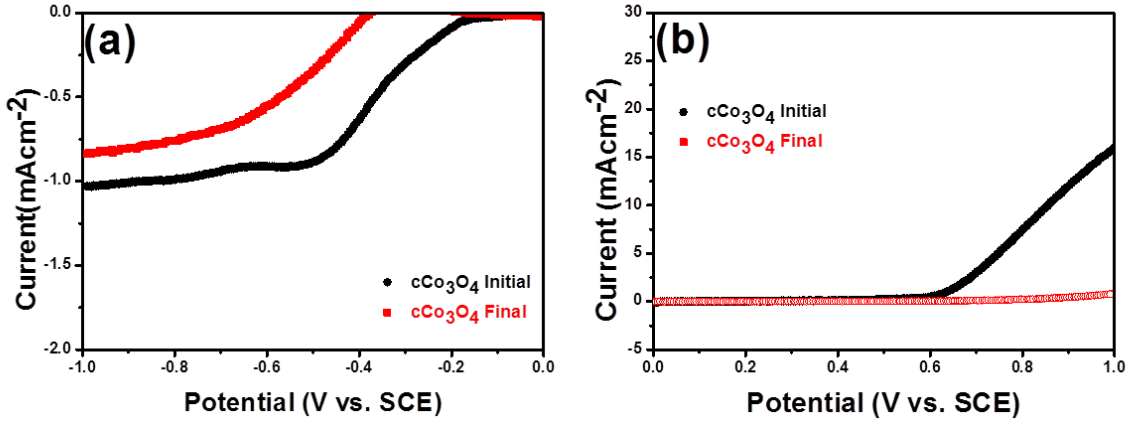

Fig.24. ORR (a) and OER (b) performance before and after CV cycling at 900rpm

Lanthanum nickelate with the addition of various portion of Vulcan carbon during synthesis has been prepared. The addition of Vulcan carbon is able to hinder the agglomeration of solid particles during heating. SEM images in Fig. 25(a), (b) and (c) indicate a clear particle size difference of lanthanum nickelate with the increasing amount of Vulcan carbon added during the synthesis (LNO-0 to LNO-2). Increasing the carbon amount addition during synthesis will lead to the formation of finer particles.However, LNO-2has only slightly smaller particle size compared to LNO-1from the SEMimages, possibly indicating little influence on morphology with excess addition of Vulcan carbon beyond this point.

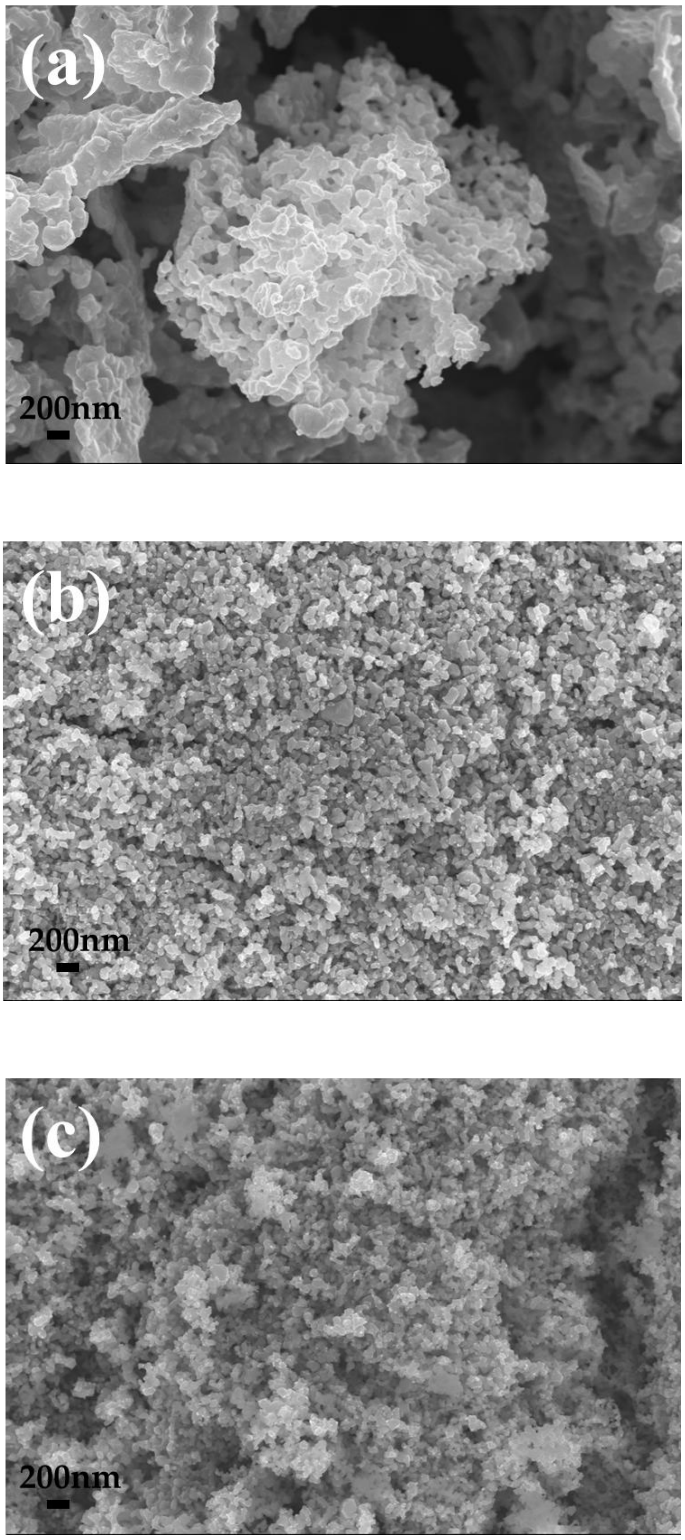

Fig.25. SEM images of LNO-0 (a), LNO-1 (b), LNO-2 (c)

To investigate the influence of particle size on the catalytic activities of lanthanum nickelate, RDE was conducted on LNO-0 and LNO-1 and the initial performance are shown in Fig.26(a) and (b). The performance of LNO-2 was not evaluated in this case primarily because the close particle size of LNO-2 and LNO-1 therefore the morphology related catalytic activity is hard to realize when comparing these two materials. Lanthanum nickelate with finer particle size such as LNO-1 demonstrated higher performance in terms of limiting current than LNO-1 which has larger particles size. The ORR limiting current of LNO-1 is higher than that of LNO-0 by 40% and the OER limiting current of LNO-1 is almost tripled that of LNO-0. As surface area is a critical factor governing electrocatalyst activity[101], decreasing the particle size of the catalyst material allows more active sites exposed at triple phase boundary thus increasing the catalytic activity.

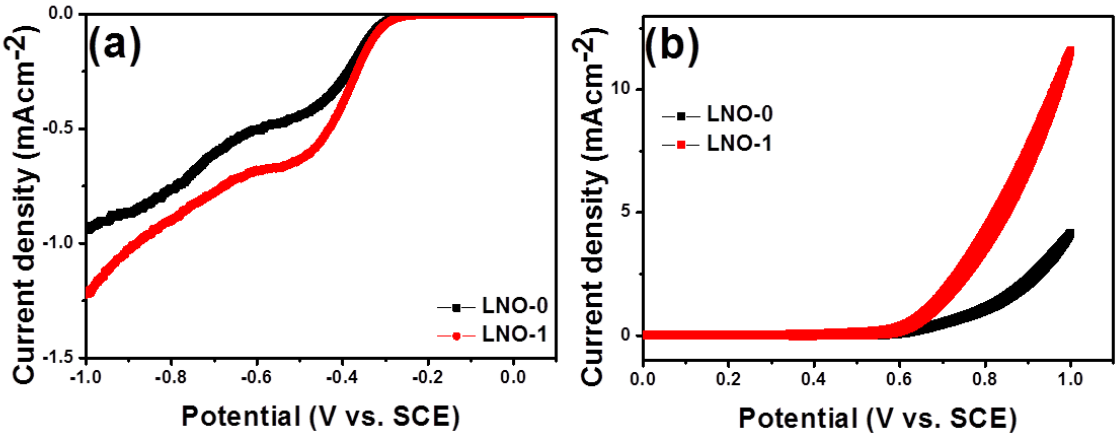

Fig.26. The initial ORR and OER performance of LNO-0 and LNO-1 measured at 900rpm

3.3.2 Summary and Conclusion

This section explores the catalytic activities of spinel cobalt oxide and perovskite lanthanum nickelate by tuning their morphologies. The morphology related performance was demonstrated

through RDE and particularly in the case of lanthanum nickelate. By increasing the amount of Vulcan carbon addition during the catalyst preparation, a deceased particle size of lanthanum nickelate was observed and a simultaneously increased ORR/OER catalytic activity was confirmed via RDE testing. Through the research described in this section, two critical aspects of catalytic activities are realized: since spinels and perovskites are semiconductors which lack of good electric conductivity for fast electron transport. Presumably,this property limits their ORR/OER catalytic activity[87]. Secondly, large surface area (or small particle size) is beneficial to obtain higher performance presumably due to larger number of active sites available for the evolution and reduction of oxygen. Further research on solving those issues is reported in the following sections by studying hybrid bifunctional catalysts.

3.4 Cubic Spinel Cobalt Oxide/Exfoliated and Nitrogen-doped Graphene

3.4.1 Results and discussions

The size, morphology and crystal structure of cCo_3O_4 has been shown in Fig. 23(a) and (b) of section 3.3.1. SEM characterizations were adopted to investigate the morphology of exfoliated and nitrogen-doped graphene and XPS was employed to obtain the surface elemental information. In Fig, 27 (a), the SEM image illustrates the formation of kinks on graphene sheet by exfoliation. Through the XPS analysis, the surface nitrogen content of ExNG is approximately 5.4% according to the XPS analysis.

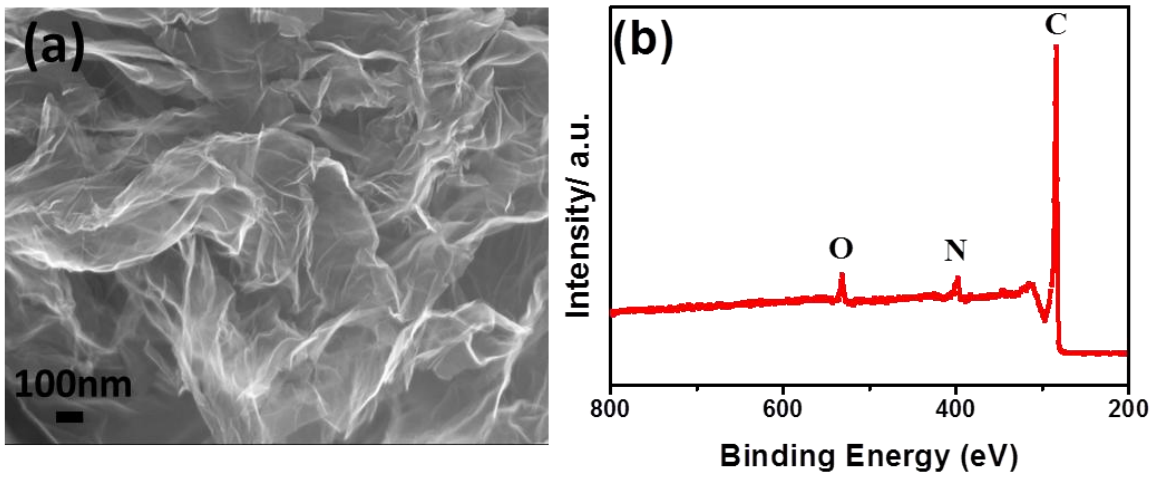

Fig.27. SEM image of ExNG (a); XPS spectrum of ExNG (b)

The bifunctional catalytic activities of cCo_3O_4, ExNG and their hybrid were evaluated in RDE. Based on the voltammetry results, a significant positive shift (+0.16V) in half-wave potential and tripled limiting current were observed in the case of the hybrid compared to the pure cobalt oxide. The tremendous enhancements in half cell performance observed for the hybrid can be attributed to the higher electrical conductivity as a consequence of ExNG addition as suggested by [35, 76, 87, 99]. Using high surface area carbon as a support for the catalysts has been investigated where the performance was drastically increased as shown from the RDE results in Fig. 28(a) and (b). Moreover, the ExNG has been widely studied as an excellent ORR catalyst itself for metal-air battery applications and combing cobalt oxide with NG further improves the ORR activity of cobalt oxide. On the other hand, spinel cobalt oxide has been reported as potential candidates for ORR and OER[10, 11]. cCo_3O_4/ExNG hybrid has been studied that showed higher activities than each of its component due to presumable synergistic effect between the cobalt oxide and graphene support. Besides the high ORR catalytic activity of the hybrid, its OER activity is also

evaluated in comparison to each of its component. The hybrid demonstrated the highest OER limiting current compared to the others. By combing cCo_3O_4 and ExNG, the limiting current of the hybrid exceeds that of cCo_3O_4 by ca. 33% and four-fold that of the ExNG.

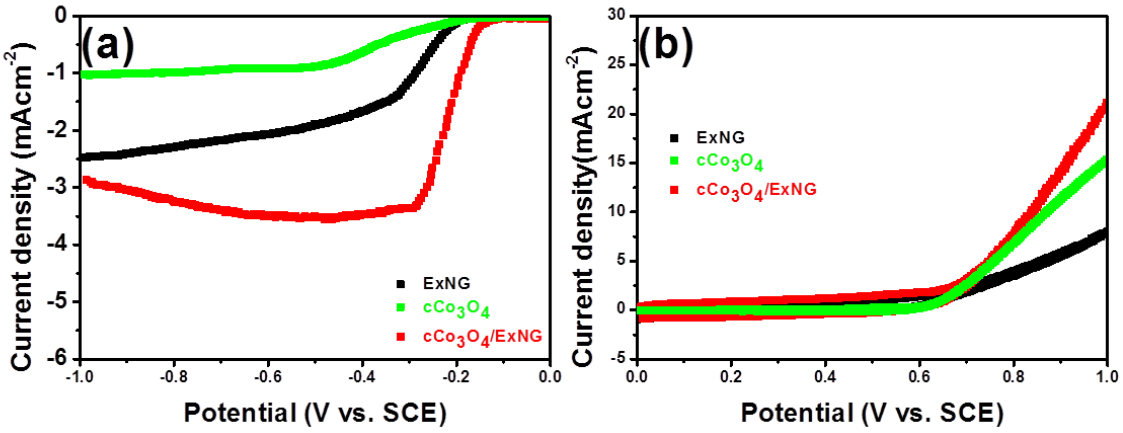

Fig.28. ORR (a) and OER (b) performance comparisons of ExNG, cCo3O4 and cCo3O4/ExNG at 900rpm

The kinetic current densities of ExNG, cCo_3O_4 and cCo_3O_4/ExNG were compared by extrapolation the Koutechy-levich plots (Fig. 29.) to the y-axis at -0.4V. The kinetic current density at -0.4V for cCo_3O_4/ExNG is 15.9 $mAcm^{-2}$ which is roughly 4 times the kinetic current density of the ExNG (3.8 $mAcm^{-2}$) and over 10 times greater than that of cCo_3O_4 (1.1 $mAcm^{-2}$). The results of K-L analysis further emphasize the benefits of using cCo_3O_4/ExNG as bifunctional catalyst for rechargeable Zn-air battery.

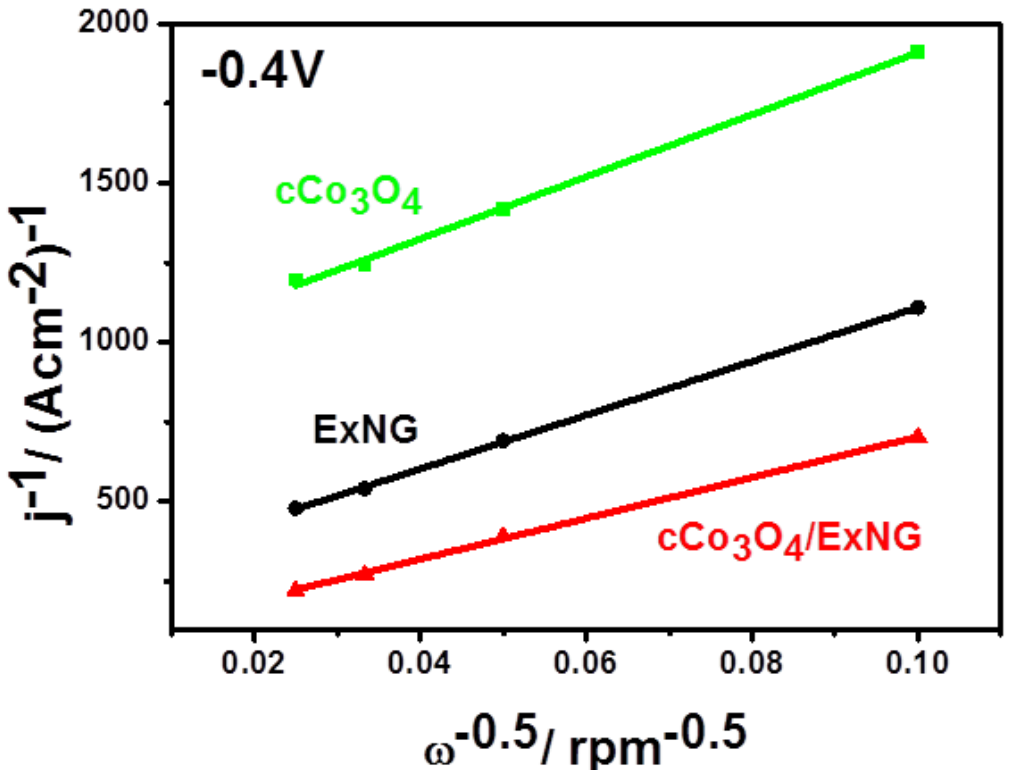

Fig.29. Koutechy-Levich plot of ExNG, cCo3O4 and cCo3O4/ExNG at -0.4V

Based on the promising results from RDE, further performance evaluation in Zn-air battery was conducted.The cell configurations and catalyst loadings were shown in the Material Characterization Techniques section. The polarization curves for battery discharge illustrates an activation loss region followed by a pseudo-linear ohmic loss region. Evidently, the hybrid exhibits lower ohmic loss compared to each of its component as shown in Fig. 30(a). The lower ohmic loss experienced by the hybrid contributes to the improvement in discharge current density. With respect to battery charging also shown in Fig. 24(a), slightly lowervoltage of the hybrid at 200mA current was observed compared to cCo_3O_4

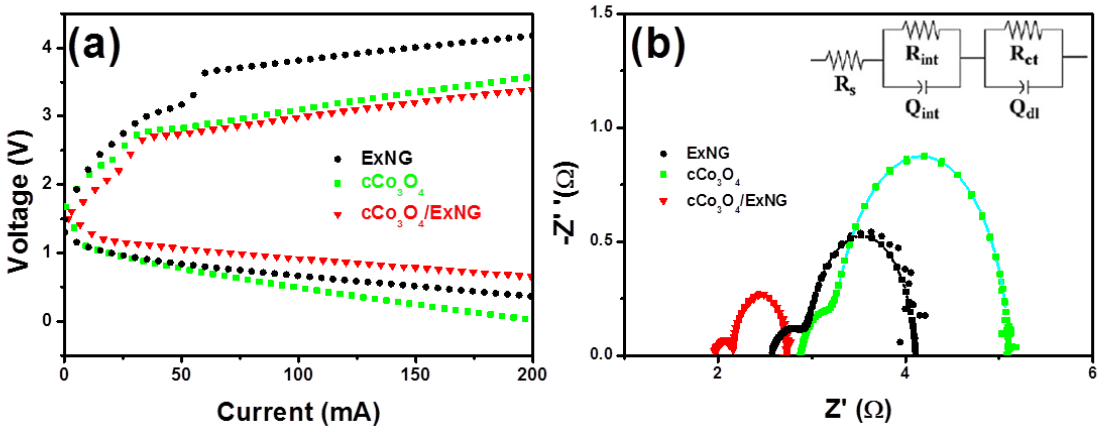

Fig.30. Charge and discharge polarizations of ExNG, cCo_3O_4 and cCo_3O_4/ExNG (a); Nyquist plot of the ExNG, cCo_3O_4 and cCo_3O_4/ExNG with the equivalent circuit of the Nyquist plots insetted.

To further understand the electrode processes of the air electrode, electrochemical impedance spectroscopy was performed. The Nyquist plots for all three catalysts illustrate two semicircles at high and low frequency regions. To identify the resistance and electrode processes of the battery, the impedance data was fitted using the equivalent circuit showed in Fig 30(b). Five elements are shown in the equivalent circuit, R_s, Q_{int}, R_{int}, Q_{dl} and R_{ct}. Similar equivalent circuit has been proposed by various researchers to investigate the electrode processes of the air electrode for zinc air battery[97, 102]. The R_s component of the equivalent circuit represents the resistance associated with various battery components, such as the electrolyte and contact resistances. The solid to electrolyte interface resistance can be present in the battery and is illustrated by R_{int}. R_{ct} represents the charge transfer resistance encountered during electrochemical reactions on the electrode. The constant phase elements, Q_{int} and Q_{dl} are included in the equivalent circuit for modeling the non-faradaic processes. The electrochemical data from the impedance spectroscopy is tabulated in Table .7 The charge transfer resistance of the hybrid is ca. one third of cCo_3O_4 and

roughly only one half of ExNG which suggests a more efficient electrocatalysis of the hybrid on the air electrode than cCo_3O_4 and ExNG.

Table 7 Equivalent circuit elements and their respective values for the air electrodes coated with ExNG, cCo3O4 and cCo3O4/ExNG.

Material	R_s	R_{int}	R_{ct}	Q_{int}	Q_{dl}
ExNG	**2.56**	**0.4375**	**1.11**	**0.00082**	**0.0181**
cCo3O4	**2.88**	**0.3932**	**1.83**	**0.023**	**0.00634**
cCo3O4/ExNG	**1.96**	**0.2108**	**0.565**	**0.037**	**0.0552**

3.4.2 Summary and Conclusion

This work explored the potential catalytic applications of cCo_3O_4/ExNG hybrid in rechargeable Zn-air batteries and the feasibility of the simplistic preparation of bifunctional catalysts. The hybrid demonstrated higher catalytic activity than each of its components in both RDE and zinc air call evaluations. This work serves as a preliminary investigation of bifunctional catalysts. The success of this system motivated the further exploration of novel low-cost hybrid materials as sustainable and efficient bifunctional catalysts, which are crucial for the widespread application of energy generation and storage devices.

3.5 Cubic Spinel Cobalt Oxide/Multi-walled Carbon Nanotubes

3.5.1 Results and Discussion

The XRD patterns of cCo_3O_4 and cCo_3O_4/MWCNT shown in Fig. 31(a) with major peaks labeled confirmed the formation of spinel structures. Due to the chemically attached MWCNTs, the peaks of cCo_3O_4 in the hybrid material were slightly shifted to larger 2θ angle compared with pure cCo_3O_4. The amount of cCo_3O_4 in the final hybrid was ~54% by mass measured by TGA and shown in Fig. 31(b). The SEM/TEM images of cCo_3O_4/MWCNT and pure cCo_3O_4 in Fig. 32(a, b, d) demonstrated the successful synthesis of cubic morphology and Fig. 32(c) shows the attached MWCNT to cCo_3O_4 surface. During the chemical reaction, the acid-functionalized MWCNTs serve as oxidizing/structure directing agents which oxidize cobalt ions to spinel cobalt oxide with functionalized carboxylate groups while regulating the formation of cubic cobalt oxide. It is demonstrated that under mild acidic conditions, the chemical modification is limited mostly to the ends of the carbon nanotubes[103]. As a result, the ends of MWCNTs are functionalized with a higher density of carboxylate groups in comparison to the nanotube walls. Consequently, the acid-functionalized MWCNTs possessed a surfactant-like structure with the relative hydrophobic part being the walls of carbon nanotubes while the hydrophilic portion residing at the ends, thus regulating the growth of cobalt oxide.

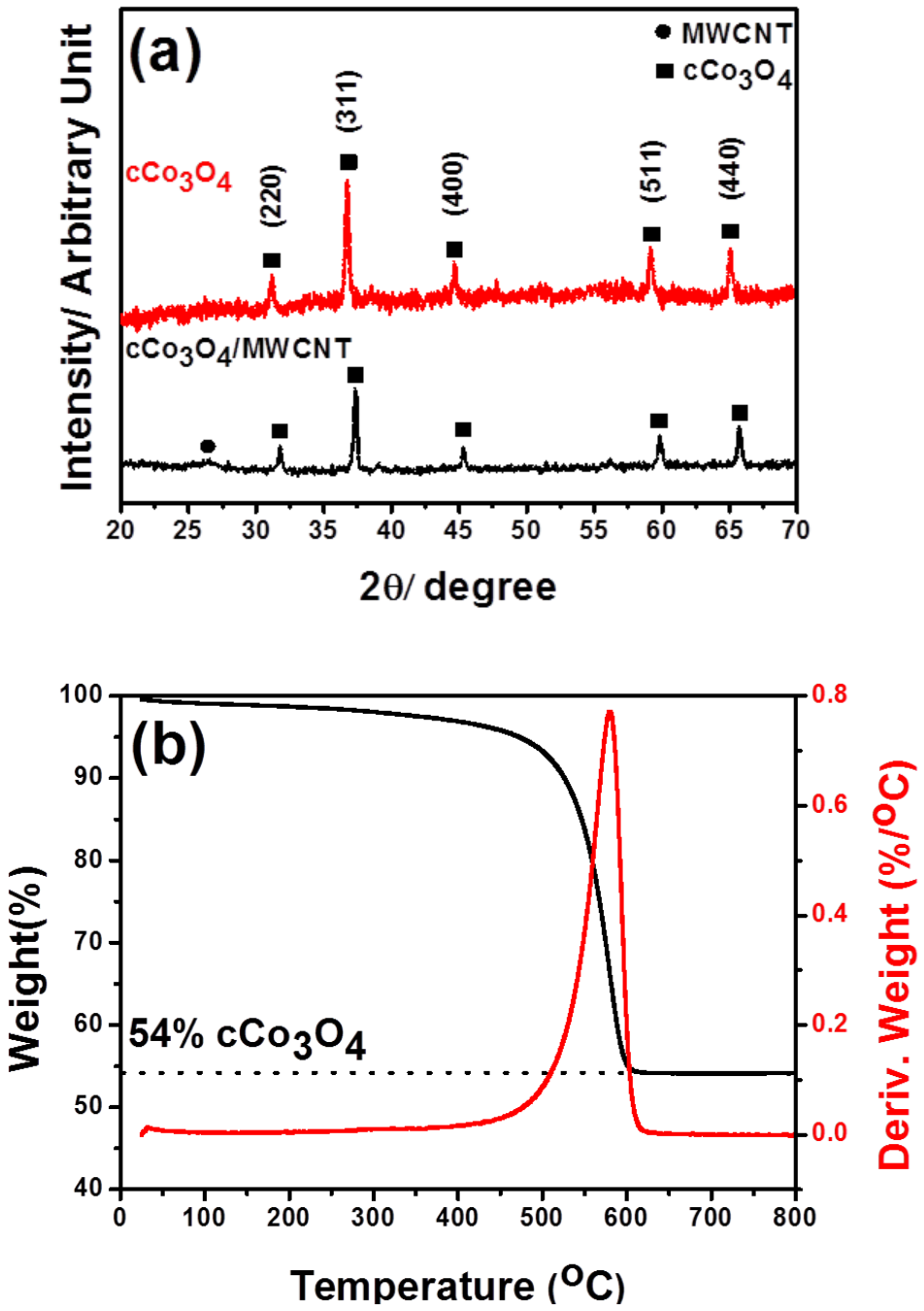

Fig.31. (a) XRD patterns of cCo3O4 and cCo3O4/MWCNT (b) TGA of cCo3O4/MWCNT

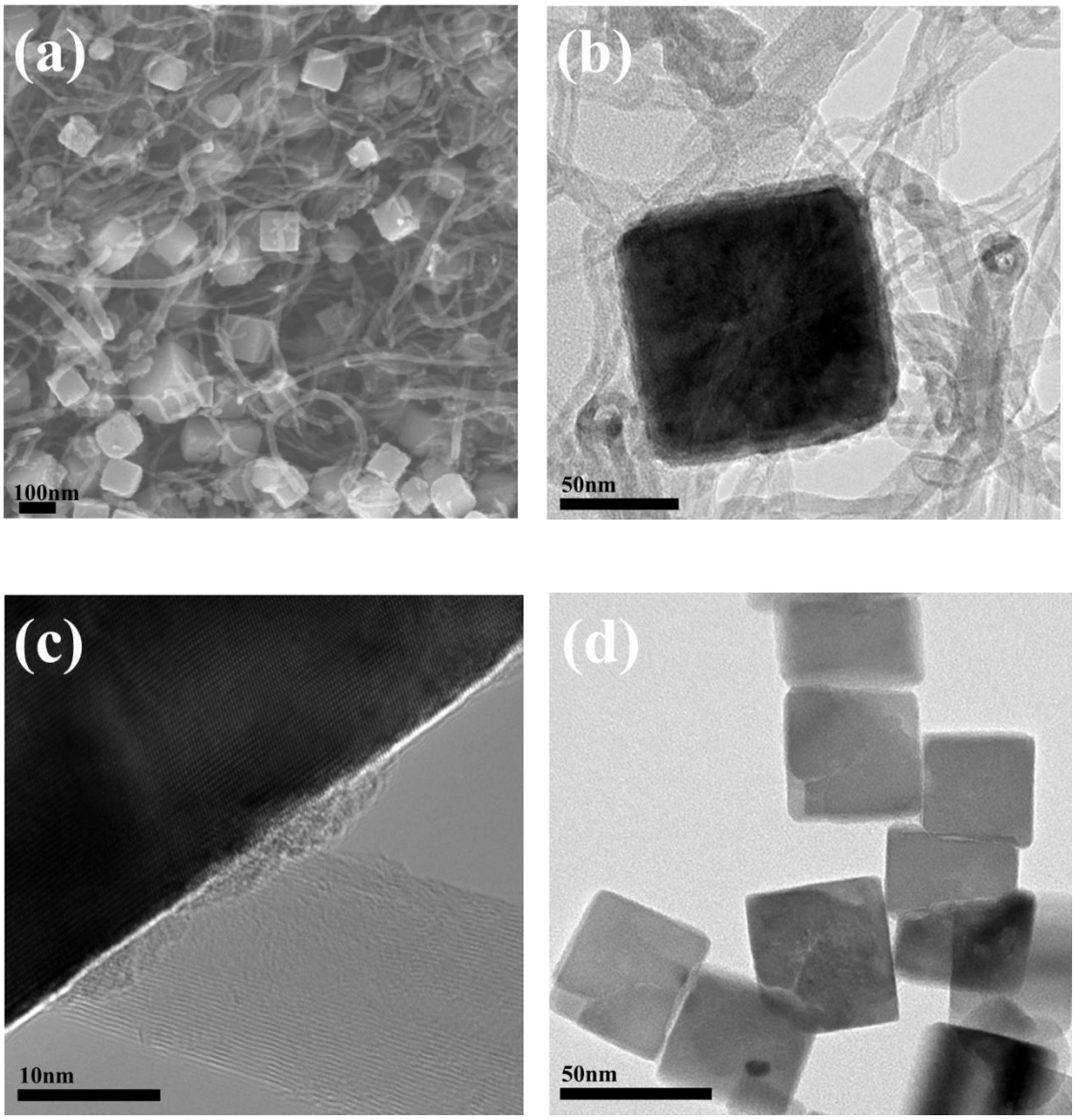

Fig.32. SEM (a) and TEM (b) images of cCo3O4 /MWCNT; HRTEM images of cCo3O4 /MWCNT (c); TEM image of pure cCo3O4 (d)

The ORR polarization curves for cCo_3O_4/MWCNT at different rotation speeds are shown in Fig.33(a). The relationship between ORR current and rotation speed is given by Koutecky-Levich equation which is plotted and shown in Fig. 33(b) with an approximate four-electron reduction pathway. The ORR/OER performance of cCo_3O_4/MWCNT was further compared to

those of MWCNT, cCo_3O_4 and the physical mixture of MWCNT and cCo_3O_4. In terms of electrochemical performance, the ORR activity of cCo_3O_4/MWCNT outperformed others showing the highest onset potential (-0.15V) and current density (-2.91 $mAcm^{-2}$ at -0.4V) in Fig 33(c). Pure cCo_3O_4 displayed very poor ORR activity while MWCNT alone showed some ORR activity, however a significantly lower onset potential (-0.20V) and the current density (-1.82 $mAcm^{-2}$ at -0.4V) than the hybrid material. The physical mixture showed improved activity compared with each component alone but was still inferior to the hybrid in ORR activity with an onset potential of -0.20V and current density of -2.22 $mAcm^{-2}$ at -0.4V. The much higher ORR performance of the hybrid material over each of its component and the physical mixture suggests that the strong coupling effect, potentially arising from the extra electron transfer pathways provided by the highly conductive MWCNT, is responsible for the outstanding ORR activity. Apart from high ORR performance, the hybrid material also exhibited excellent OER activity exhibiting the highest current density (29.5 $mAcm^{-2}$ at 1V) in comparison to each component alone and the physical mixture as shown in Fig. 33(d).

While the ORR and OER performance are the most commonly evaluated parameters for bifunctional catalysts, the stability of electrocatalysts is also of practical importance. Typically, carbon-composed electrocatalysts are prone to degradation caused by surface oxidation after long periods of operation. To investigate the stability of catalysts, cyclic voltammetry (CV) cycling was performed in the RDE system. For the hybrid material, it retained high bifunctionality following CV cycling. The ORR onset potential of the hybrid remained the same over continuous cycling and the current density decreased by only 23%. In the case of MWCNT, cCo_3O_4 and the physical mixture, severe ORR performance degradation in terms of onset potential and current density was observed after 500 cycles. After cycling, the ORR current

density of the hybrid shows 3.7, 34 and 3 times greater than that of MWCNT, cCo_3O_4 and the physical mixture, respectively. Moreover, the MWCNT and cCo_3O_4 suffered from significant OER degradation after cycling (92% and 94%, respectively) whereas the hybrid material demonstrated an outstanding stability with only 15% of performance decrease, which is also far more superior to the physical mixture (30% higher current density). A direct performance comparison of all the catalysts before and after cycling is summarized in Table 8.These electrochemical results indicate that the oxidation of the MWCNTs was not prevalent and the unique structure potentially strengthens the overall stability of the hybrid. Furthermore, the synergistic coupling effect could exist between cCo_3O_4 and MWCNT and the enhanced stability of the attached MWCNT could be affected by cCo_3O_4 in the hybrid assisting the prevention of carbon corrosion[35]. These results made our hybrid material a high performance non-precious metal-based bifunctional electrocatalyst.

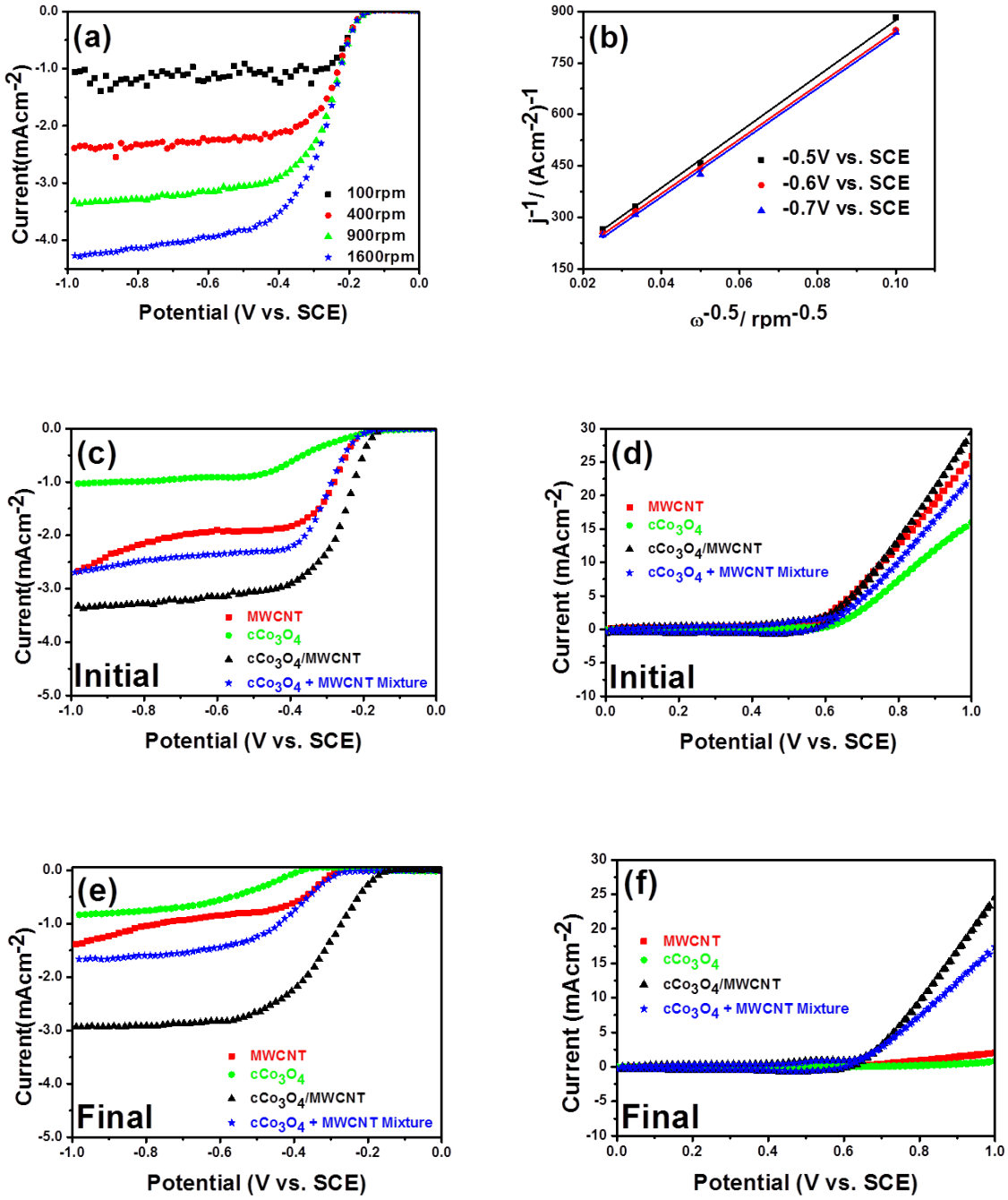

Fig.33. (a) ORR polarization curve of cCo3O4/MWCNT at various rotation speeds; (b) Koutecky-levich plots of cCo3O4/MWCNT at -0.5V, -0.6V and -0.7V; Initial ORR (c)/OER (d) and final ORR (e)/OER (d) polarization curves of MWCNT, cCo3O4, cCo3O4/MWCNT, cCo3O4 + MWCNT Mixture

Table 8 Summarized ORR/OER results of MWCNT, cCo3O4, cCo3O4/MWCNT and cCo3O4 + MWCNT Mixture.

	Initial Performance		Final Performance	
Catalysts Evaluated	**ORR current density ($mAcm^{-2}$) at -0.4V vs. SCE**	**OER current density ($mAcm^{-2}$) at 1v vs. SCE**	**ORR current density ($mAcm^{-2}$) at -0.4V vs. SCE**	**OER current density ($mAcm^{-2}$) at 1v vs. SCE**
MWCNT	**-1.82**	**25.6**	**-0.607**	**2.09**
cCo_3O_4	**-0.650**	**15.9**	**-0.0650**	**0.82**
cCo_3O_4/MWCNT	**-2.91**	**29.5**	**-2.24**	**24.6**
cCo_3O_4 + MWCNT Mixture	**-2.22**	**22.6**	**-0.759**	**17.3**

3.5.2 Summary and Conclusion

The bifunctional electrocatalyst cCo_3O_4/MWCNT has been successfully prepared via a facile hydrothermal method. This hybrid material demonstrated much higher bifunctionality and stability over its individual components and the physical mixture, which could potentially be a result of the synergistic effect between each component of the hybrid material. Further investigations on how the interaction between MWCNT and cubic spinel cobalt oxide influences the catalytic activities are proposed. Based upon the promising results, the non-precious metal-

based hybrid material could facilitate the large-scale implementations of rechargeable metal-air batteries.

3.6 Discussion and Comparison of the Studied Catalysts

In comparison of the ORR activity, the activated and nitrogen doped carbon nanofibres demonstrated moderate ORR performance, but among all the catalysts studied in this work, it is able to be synthesized with the easiest method. Spinel cobalt oxide and perovskite lanthanum nickelate have low ORR activity, presumably because of the low intrinsic conductivities. Reducing the particle size of lanthanum nickelate by modifying synthesis procedures leads to increase of ORR and OER limiting current density indicating the importance of material morphology, but their bifunctional catalytic activities still much lower than other catalysts studied. Physically mixing spinel cobalt oxide with exfoliated and nitrogen-doped graphene gave much higher bifunctional catalytic activities than each of its component suggesting that the conductivity of metal oxides as electrocatalyst is significant. However due to the limited interaction between the metal oxide and graphene, the performance of the cubic cobalt oxide and exfoliated and nitrogen-doped graphene hybrid is not as good as the cobalt oxide chemically attached onto the carbon nanotube. In general, in order to have high efficient bifunctional catalyst of this type, close attachment of the metal oxide onto the carbon substrate is the key for high performance bifunctional catalyst.

CHAPTER 4: Conclusions and Recommendations

4.1 Conclusions

Three types of catalysts have been synthesized and evaluated ranging from carbon nanofibres, spinel cobalt oxide and perovskite lanthanum nickelate.Understanding their chracteristics eventually lead to the synthesis of hybrid catalysts like cobalt oxide with graphene and carbon nanotubes. In the first study, the commercial carbon nanofibre undergoes alkaline activation and nitrogen-doping at selected temperature and the highest catalytic activity was found at 950˚C activation temperature. KOH activation and ammonia nitrogen-doping increased the ORR performance of pristine CNF by ~17% and ~40% in terms of limiting current and onset potential, respectively. Although the ORR performance of a(950)-NCNF was not outstanding, the low cost of CNF among carbon materials and the simplistic post-treatment processes still make CNF an excellent candidate for ORR catalysis and worth in-depth research to realize its vast potential. In the second study, the cubic structure of spinel cobalt oxide and lanthanum nickelate with small particle size was successfully synthesized. The cubic spinel cobalt oxide was further used in the studies of bifunctional hybrid materials. Lanthanum nickelate with small particle size was achieved via the addition of Vulcan carbon into the sol-gel synthesis process. With the presence of carbon, lanthanum nickelate is unable to agglomerate into large chunks but instead, finer particles are achievable with higher amount of carbon addition. The influence of particle sizes on the ORR and OER performance was studied with RDE testing. Decreasing particle size leads to an increase in bifunctional catalytic activity of lanthanum nickelate. This study emphasized on the importance of tuning the nanostructure of the material to obtain higher catalytic activity via modified synthesis process. The studies on carbonaceous materials and structured metal oxides laid a strong foundation for the following research on the hybrid bifunctional catalysts.

Physically mixing spinel cobalt oxide with ExNG provides a conducting surface for the spinel cobalt oxide. With the increase of conductivity rised from the carbon surface, the bifunctional activity of cCo_3O_4/ExNG hybrid is enhanced. The hybrid demonstrated higher catalytic activity than each of its components in both RDE and Zn-air call evaluations. Nevertheless, the enhancement of the conductivity might be limited by the relatively loose interactions between the conducting surface ExNG and spinel cobalt oxide. Chemically attaching cobalt oxide onto the carbon nanotube affords strong interactions between the metal oxide and the carbon. Acid-functionalized carbon nanotubes are able to oxide the cobalt precursors present in the solution to form metal oxides on the carbon surface. The increased metal oxide/carbon connection of cCo_3O_4/MWCNT provides it the highest bifunctional catalytic activity and durability among the studied materials. An important feature of the metal oxide/carbon hybrid synthesis approach is worth emphasizing. The mildly oxidized MWCNT plays an indispensible role in the synthesis process. It has been demonstrated that under mild conditions, the chemical modification is limited mostly to the ends of the carbon nanotubes. As a result, the functionalized MWCNTs possessed a surfactant-like structure with the relative hydrophobic part being the wall of carbon nanotubes while the hydrophilic portion residing at the end[103]. The functionalized MWCNTs serve as oxidizing/structure directing agents which oxidize cobalt ions to spinel cobalt oxide with their carboxylate groups meanwhile regulate the formation of cubic cobalt oxide. The degree of oxidation of carbon is expected to afford a degree of control over the morphology of metal oxides which could provide a novel method for tuning the morphology of metal oxides by oxidized carbon. This is interesting and worth more detailed explorations

4.2 Future Work

Further work is still required in order for metal oxide/carbon hybrid bifunctional catalysts to become a successful category of electrocatalyst. In particular, a foundamental understanding of the synthesis process, material structure and properties of the hybrid nanomaterials is desirable. The interactions between oxidized carbon and metal oxides will be the main focus in the future which is the key step for fabricating the hybrid materials.The causes for the high performance and stability of metal oxides/carbon hybrid are yet not fully understood. Well- understanding the reasons behind this phenomenon would serve as a guide for the future development of bifunctional electrocatalysts with much higher activities and stabilities. Furthermore, the morphology related performance for the hybrid catalyst is still not fully understood only through the studies shown here. The acid-functionlized carbon nanotube as oxidizing and structure regulating agent is an interesting area to explore where by controlling the degree of acid-functionalization might lead different morphologies of attached metal-oxide. Spectroscopic techniques such as electron energy loss spectroscopy and x-ray absorption near edge structure spectroscopy are able to facilitate the understanding of the origin of high catalytic activities of the hybrid materials. Last but not the least, for practical applications, it is important to develop synthesis methods suitable for large scale productions. Therefore, the following specific recommendations for future study are made:

- Synthesize cCo_3O_4/MWCNT with the same procedure stated in this work but using MWCNT functionalized with various time or temperatures and focus on the changes of performance and morphologies
- Explore the uses of acid-functionlized graphene and carbon nanofibres as structure directing and oxidizing agents

- Utilize suitable spectroscopic techniques to characterize the hybrid materials aiming to explain the origin of their catalytic activities
- Develop a facile method for the synthesis of hybrid materials.

References

[1] P. Sapkota, H. Kim, Zinc–air fuel cell, a potential candidate for alternative energy, Journal of Industrial and Engineering Chemistry, 15 (2009) 445-450.

[2] O. Haas, F. Holzer, K. Müller, S. Müller, Metal/air batteries: the zinc/air case, in: Handbook of Fuel Cells, John Wiley & Sons, Ltd, 2010.

[3] D. Higgins, Z. Chen, D.U. Lee, Z. Chen, Activated and nitrogen-doped exfoliated graphene as air electrodes for metal-air battery applications, Journal of Materials Chemistry A, 1 (2013) 2639-2645.

[4] Z. Yang, Z. Yao, G. Li, G. Fang, H. Nie, Z. Liu, X. Zhou, X.a. Chen, S. Huang, Sulfur-doped graphene as an efficient metal-free cathode catalyst for oxygen reduction, ACS Nano, 6 (2011) 205-211.

[5] L. Yang, S. Jiang, Y. Zhao, L. Zhu, S. Chen, X. Wang, Q. Wu, J. Ma, Y. Ma, Z. Hu, Boron-Doped Carbon Nanotubes as Metal-Free Electrocatalysts for the Oxygen Reduction Reaction, Angewandte Chemie, 123 (2011) 7270-7273.

[6] Z.W. Liu, F. Peng, H.J. Wang, H. Yu, W.X. Zheng, J. Yang, Phosphorus-Doped Graphite Layers with High Electrocatalytic Activity for the O2 Reduction in an Alkaline Medium, Angewandte Chemie, 123 (2011) 3315-3319.

[7] Y. Liang, H. Wang, J. Zhou, Y. Li, J. Wang, T. Regier, H. Dai, Covalent Hybrid of Spinel Manganese–Cobalt Oxide and Graphene as Advanced Oxygen Reduction Electrocatalysts, Journal of the American Chemical Society, 134 (2012) 3517-3523.

[8] A.M. Kannan, A.K. Shukla, S. Sathyanarayana, Oxide-based bifunctional oxygen electrode for rechargeable metal/air batteries, Journal of Power Sources, 25 (1989) 141-150.

[9] L. Swette, N. Kackley, Oxygen electrodes for rechargeable alkaline fuel cells - II, Journal of Power Sources, 29 (1990) 423-436.

[10] H.N. Cong, K.E. Abbassi, P. Chartier, Electrocatalysis of Oxygen Reduction on Polypyrrole/Mixed Valence Spinel Oxide Nanoparticles, Journal of The Electrochemical Society, 149 (2002) A525-A530.

[11] E. Rios, J.L. Gautier, G. Poillerat, P. Chartier, Mixed valency spinel oxides of transition metals and electrocatalysis: case of the MnxCo3−xO4 system, Electrochimica Acta, 44 (1998) 1491-1497.

[12] J. Feng, H.C. Zeng, Size-Controlled Growth of Co3O4 Nanocubes, Chemistry of Materials, 15 (2003) 2829-2835.

[13] H. Wang, H. Dai, Strongly coupled inorganic-nano-carbon hybrid materials for energy storage, Chemical Society Reviews, 42 (2013) 3088-3113.

[14] R.J. Brodd, SECONDARY BATTERIES | Overview, in: G. Editor-in-Chief: Jürgen (Ed.) Encyclopedia of Electrochemical Power Sources, Elsevier, Amsterdam, 2009, pp. 254-261.

[15] M. Winter, R.J. Brodd, What Are Batteries, Fuel Cells, and Supercapacitors?, Chemical Reviews, 104 (2004) 4245-4270.

[16] G. Hoogers, Fuel cell technology handbook, CRC press, 2002.

[17] K.F. Blurton, A.F. Sammells, Metal/air batteries: Their status and potential — a review, Journal of Power Sources, 4 (1979) 263-279.

[18] F. Cheng, J. Chen, Metal-air batteries: from oxygen reduction electrochemistry to cathode catalysts, Chemical Society Reviews, 41 (2012) 2172-2192.

[19] A.F. Ghoniem, Needs, resources and climate change: Clean and efficient conversion technologies, Progress in Energy and Combustion Science, 37 (2011) 15-51.

[20] K. Kinoshita, S. Electrochemical, Electrochemical oxygen technology, Wiley, New York, 1992.

[21] A. Kraytsberg, Y. Ein-Eli, The impact of nano-scaled materials on advanced metal–air battery systems, Nano Energy.

[22] J. Wang, S. Li, S. Zhang, Novel Hydroxide-Conducting Polyelectrolyte Composed of an Poly(arylene ether sulfone) Containing Pendant Quaternary Guanidinium Groups for Alkaline Fuel Cell Applications, Macromolecules, 43 (2010) 3890-3896.

[23] B. Scrosati, J. Garche, Lithium batteries: Status, prospects and future, Journal of Power Sources, 195 (2010) 2419-2430.

[24] G. Girishkumar, B. McCloskey, A.C. Luntz, S. Swanson, W. Wilcke, Lithium−Air Battery: Promise and Challenges, The Journal of Physical Chemistry Letters, 1 (2010) 2193-2203.

[25] A. Kraytsberg, Y. Ein-Eli, Review on Li–air batteries—Opportunities, limitations and perspective, Journal of Power Sources, 196 (2011) 886-893.

[26] T. Ogasawara, A. Débart, M. Holzapfel, P. Novák, P.G. Bruce, Rechargeable Li2O2 Electrode for Lithium Batteries, Journal of the American Chemical Society, 128 (2006) 1390-1393.

[27] S.A. Freunberger, Y. Chen, N.E. Drewett, L.J. Hardwick, F. Bardé, P.G. Bruce, The Lithium–Oxygen Battery with Ether-Based Electrolytes, Angewandte Chemie International Edition, 50 (2011) 8609-8613.

[28] D. Linden, T.B. Reddy, T. Reddy, Linden's Handbook of Batteries, in, McGraw-Hill Professional, New York, 2010.

[29] S.F. Bender, J.W. Cretzmeyer, T.F. Reise, Zinc/air Cells, Handbook of Batteries, (1994) 131.

[30] J.J. Martin, V. Neburchilov, H. Wang, W. Qu, Air cathodes for metal-air batteries and fuel cells, in: Electrical Power & Energy Conference (EPEC), 2009 IEEE, 2009, pp. 1-6.

[31] S.F. Bender, J.W. Cretzmeyer, T.F. Reise, Zinc/air batteries—button configuration, Handbook of batteries, 3rd Eds. McGraw-Hill, New York, 13 (2002).

[32] H. Zarrin, J. Wu, M. Fowler, Z. Chen, High durable PEK-based anion exchange membrane for elevated temperature alkaline fuel cells, Journal of Membrane Science, 394–395 (2012) 193-201.

[33] D. Meza, D.C. Higgins, J. Wu, Z. Chen, One-Step Synthesized Tungsten Oxide/Carbon Nanotube Composites as Pt Catalyst Supports for Oxygen Reduction Reaction in Proton Exchange Membrane Fuel Cells, Journal of Nanoengineering and Nanomanufacturing, 1 (2011) 280-286.

[34] J. Wu, W. Li, D. Higgins, Z. Chen, Heat-Treated Nonprecious Catalyst Using Fe and Nitrogen-Rich 2,3,7,8-Tetra(pyridin-2-yl)pyrazino[2,3-g]quinoxaline Coordinated Complex for Oxygen Reduction Reaction in PEM Fuel Cells, The Journal of Physical Chemistry C, 115 (2011) 18856-18862.

[35] Z. Chen, A. Yu, D. Higgins, H. Li, H. Wang, Z. Chen, Highly Active and Durable Core–Corona Structured Bifunctional Catalyst for Rechargeable Metal–Air Battery Application, Nano Letters, 12 (2012) 1946-1952.

[36] I. Moussallem, J. Jörissen, U. Kunz, S. Pinnow, T. Turek, Chlor-alkali electrolysis with oxygen depolarized cathodes: history, present status and future prospects, J Appl Electrochem, 38 (2008) 1177-1194.

[37] Y. Liang, Y. Li, H. Wang, H. Dai, Strongly Coupled Inorganic/Nanocarbon Hybrid Materials for Advanced Electrocatalysis, Journal of the American Chemical Society, 135 (2013) 2013-2036.

[38] M.T.M. Koper, Thermodynamic theory of multi-electron transfer reactions: Implications for electrocatalysis, Journal of Electroanalytical Chemistry, 660 (2011) 254-260.

[39] M.W. Kanan, D.G. Nocera, In Situ Formation of an Oxygen-Evolving Catalyst in Neutral Water Containing Phosphate and Co2+, Science, 321 (2008) 1072-1075.

[40] J.P. Zheng, R.Y. Liang, M. Hendrickson, E.J. Plichta, Theoretical Energy Density of Li–Air Batteries, Journal of The Electrochemical Society, 155 (2008) A432-A437.

[41] E.G. Dow, The development of aluminum aqueous batteries for torpedo propulsion: prototype development of a replenishment electrolyte management system for activation and control of a pile configured battery cartridge, in: Battery Conference on Applications and Advances, 1996., Eleventh Annual, 1996, pp. 61-66.

[42] C. Lan, T. Chin, P. Lin, T. Wang, P. Sebastian, A. Millan, P. Parkhutik, S. Gamboa, Zn-Al alloy as a new anode-metal of a zinc-air battery, Journal of New Materials for Electrochemical Systems, 9 (2006) 27.

[43] A. Dobley, C. Morein, R. Roark, Lithium-Air Cells with High Capacity Cathodes, ECS Transactions, 3 (2008) 83-88.

[44] O.V. Roussak, H.D. Gesser, Electrochemistry, Batteries, and Fuel Cells, in: Applied Chemistry, Springer US, 2013, Ch. 9, pp. 145-173.

[45] R.M. Dell, Batteries: fifty years of materials development, Solid State Ionics, 134 (2000) 139-158.

[46] Z. Chen, Nitrogen-Doped Carbon Materials as Oxygen Reduction Reaction Catalysts for Metal-Air Fuel Cells and Batteries, (2012).

[47] A.R. Suresh Kannan, S. Muralidharan, K.B. Sarangapani, V. Balaramachandran, V. Kapali, Corrosion and anodic behaviour of zinc and its ternary alloys in alkaline battery electrolytes, Journal of Power Sources, 57 (1995) 93-98.

[48] C.-C. Yang, S.-J. Lin, Improvement of high-rate capability of alkaline Zn–MnO2 battery, Journal of Power Sources, 112 (2002) 174-183.

[49] X.G. Zhang, Fibrous zinc anodes for high power batteries, Journal of Power Sources, 163 (2006) 591-597.

[50] B. Szcześniak, M. Cyrankowska, A. Nowacki, Corrosion kinetics of battery zinc alloys in electrolyte solutions, Journal of Power Sources, 75 (1998) 130-138.

[51] N.M. Marković, P.N. Ross Jr, Surface science studies of model fuel cell electrocatalysts, Surface Science Reports, 45 (2002) 117-229.

[52] J. Zhu, Y. Zhou, C. Gao, Influence of surfactants on electrochemical behavior of zinc electrodes in alkaline solution, Journal of Power Sources, 72 (1998) 231-235.

[53] M. Yano, S. Fujitani, K. Nishio, Y. Akai, M. Kurimura, Effect of additives in zinc alloy powder on suppressing hydrogen evolution, Journal of Power Sources, 74 (1998) 129-134.

[54] E. Fraçkowiak, J.M. Skowroński, Passivation of zinc in alkaline solution effected by chromates and CrO3-graphite system, Journal of Power Sources, 73 (1998) 175-181.

[55] C.W. Lee, K. Sathiyanarayanan, S.W. Eom, H.S. Kim, M.S. Yun, Effect of additives on the electrochemical behaviour of zinc anodes for zinc/air fuel cells, Journal of Power Sources, 160 (2006) 161-164.

[56] C.W. Lee, K. Sathiyanarayanan, S.W. Eom, M.S. Yun, Novel alloys to improve the electrochemical behavior of zinc anodes for zinc/air battery, Journal of Power Sources, 160 (2006) 1436-1441.

[57] J. Kan, H. Xue, S. Mu, Effect of inhibitors on Zn-dendrite formation for zinc-polyaniline secondary battery, Journal of Power Sources, 74 (1998) 113-116.

[58] P. Sapkota, H. Kim, An experimental study on the performance of a zinc air fuel cell with inexpensive metal oxide catalysts and porous organic polymer separators, Journal of Industrial and Engineering Chemistry, 16 (2010) 39-44.

[59] D. Tang, J. Pan, S. Lu, L. Zhuang, J. Lu, Alkaline polymer electrolyte fuel cells: Principle, challenges, and recent progress, Sci. China Chem., 53 (2010) 357-364.

[60] P. Arora, Z. Zhang, Battery separators, Chemical Reviews-Columbus, 104 (2004) 4419-4462.

[61] G.M. Wu, S.J. Lin, J.H. You, C.C. Yang, Study of high-anionic conducting sulfonated microporous membranes for zinc-air electrochemical cells, Materials Chemistry and Physics, 112 (2008) 798-804.

[62] E.L. Dewi, K. Oyaizu, H. Nishide, E. Tsuchida, Cationic polysulfonium membrane as separator in zinc–air cell, Journal of Power Sources, 115 (2003) 149-152.

[63] M. Armand, J.-M. Tarascon, Building better batteries, Nature, 451 (2008) 652-657.

[64] M. Kar, B. Winther-Jensen, M. Forsyth, D.R. MacFarlane, Chelating ionic liquids for reversible zinc electrochemistry, Physical Chemistry Chemical Physics, (2013).

[65] Y.-G. Guo, J.-S. Hu, L.-J. Wan, Nanostructured Materials for Electrochemical Energy Conversion and Storage Devices, Advanced Materials, 20 (2008) 2878-2887.

[66] A. Manthiram, A. Vadivel Murugan, A. Sarkar, T. Muraliganth, Nanostructured electrode materials for electrochemical energy storage and conversion, Energy & Environmental Science, 1 (2008) 621-638.

[67] B. Scrosati, J. Hassoun, Y.-K. Sun, Lithium-ion batteries. A look into the future, Energy & Environmental Science, 4 (2011) 3287-3295.

[68] O.K. Park, Y. Cho, S. Lee, H.-C. Yoo, H.-K. Song, J. Cho, Who will drive electric vehicles, olivine or spinel?, Energy & Environmental Science, 4 (2011) 1621-1633.

[69] J. Goldstein, I. Brown, B. Koretz, New developments in the Electric Fuel Ltd. zinc/air system, Journal of Power Sources, 80 (1999) 171-179.

[70] K.T. Chau, Y.S. Wong, C.C. Chan, An overview of energy sources for electric vehicles, Energy Conversion and Management, 40 (1999) 1021-1039.

[71] “Electrical energy storage technology options” (Report 1020676, Electric Power Research Institute, Palo Alto, CA, December 2010)

[72] " Preliminary Analysis of eVionyx Ni-Zn battery and Zn-air Fuel Cell” (Report prepared by Electric Mobility Canada, Mississauga, ON, Canada, December 2006)

[73] W.W. Clark Ii, E. Paolucci, J. Cooper, Commercial development of energy - Environmentally sound technologies for the auto-industry: The case of fuel cells, Journal of Cleaner Production, 11 (2003) 427-437.

[74] Johnson Matthey, Price of Platinum Metal (http://www.platinum.matthey.com) acessesd March, 2013

[75] T. Martins, R. Miwa, A.J. da Silva, A. Fazzio, Electronic and transport properties of boron-doped graphene nanoribbons, Physical review letters, 98 (2007) 196803.

[76] Y. Liang, Y. Li, H. Wang, J. Zhou, J. Wang, T. Regier, H. Dai, Co3O4 nanocrystals on graphene as a synergistic catalyst for oxygen reduction reaction, Nat Mater, 10 (2011) 780-786.

[77] N.M. Rodriguez, A review of catalytically grown carbon nanofibers, Journal of Materials Research, 8 (1993) 3233-3250.

[78] S.-H. Yoon, S. Lim, Y. Song, Y. Ota, W. Qiao, A. Tanaka, I. Mochida, KOH activation of carbon nanofibers, Carbon, 42 (2004) 1723-1729.

[79] H. Marsh, D.S. Yan, T.M. O'Grady, A. Wennerberg, Formation of active carbons from cokes using potassium hydroxide, Carbon, 22 (1984) 603-611.

[80] P. Ehrburger, A. Addoun, F. Addoun, J.-B. Donnet, Carbonization of coals in the presence of alkaline hydroxides and carbonates: formation of activated carbons, Fuel, 65 (1986) 1447-1449.

[81] T. Otowa, Y. Nojima, T. Miyazaki, Development of KOH activated high surface area carbon and its application to drinking water purification, Carbon, 35 (1997) 1315-1319.

[82] D. Lozano-Castello, M. Lillo-Rodenas, D. Cazorla-Amoros, A. Linares-Solano, Preparation of activated carbons from Spanish anthracite: I. Activation by KOH, Carbon, 39 (2001) 741-749.

[83] A. Ahmadpour, D. Do, The preparation of active carbons from coal by chemical and physical activation, Carbon, 34 (1996) 471-479.

[84] N. Yoshizawa, K. Maruyama, Y. Yamada, E. Ishikawa, M. Kobayashi, Y. Toda, M. Shiraishi, XRD evaluation of KOH activation process and influence of coal rank, Fuel, 81 (2002) 1717-1722.

[85] M. Lillo-Ródenas, D. Cazorla-Amorós, A. Linares-Solano, Understanding chemical reactions between carbons and NaOH and KOH: an insight into the chemical activation mechanism, Carbon, 41 (2003) 267-275.

[86] Y. Zhu, S. Murali, M.D. Stoller, K.J. Ganesh, W. Cai, P.J. Ferreira, A. Pirkle, R.M. Wallace, K.A. Cychosz, M. Thommes, D. Su, E.A. Stach, R.S. Ruoff, Carbon-Based Supercapacitors Produced by Activation of Graphene, Science, 332 (2011) 1537-1541.

[87] L. Wang, X. Zhao, Y. Lu, M. Xu, D. Zhang, R.S. Ruoff, K.J. Stevenson, J.B. Goodenough, CoMn2O4 spinel nanoparticles grown on graphene as bifunctional catalyst for lithium-air batteries, Journal of The Electrochemical Society, 158 (2011) A1379-A1382.

[88] Y. Liang, H. Wang, P. Diao, W. Chang, G. Hong, Y. Li, M. Gong, L. Xie, J. Zhou, J. Wang, T.Z. Regier, F. Wei, H. Dai, Oxygen Reduction Electrocatalyst Based on Strongly Coupled Cobalt Oxide Nanocrystals and Carbon Nanotubes, Journal of the American Chemical Society, 134 (2012) 15849-15857.

[89] E.J. Crumlin, S.-J. Ahn, D. Lee, E. Mutoro, M.D. Biegalski, H.M. Christen, Y. Shao-Horn, Oxygen Electrocatalysis on Epitaxial La0. 6Sr0. 4CoO3-δ Perovskite Thin Films for Solid Oxide Fuel Cells, Journal of The Electrochemical Society, 159 (2012) F219-F225.

[90] Y. Li, S. Yao, W. Wen, L. Xue, Y. Yan, Sol–gel combustion synthesis and visible-light-driven photocatalytic property of perovskite LaNiO3, Journal of Alloys and Compounds, 491 (2010) 560-564.

[91] J.D.G. Fernandes, D.M.A. Melo, L.B. Zinner, C.M. Salustiano, Z.R. Silva, A.E. Martinelli, M. Cerqueira, C. Alves Júnior, E. Longo, M.I.B. Bernardi, Low-temperature synthesis of single-phase crystalline LaNiO3 perovskite via Pechini method, Materials Letters, 53 (2002) 122-125.

[92] S. Zhuang, C. Huang, K. Huang, X. Hu, F. Tu, H. Huang, Preparation of homogeneous nanoporous La0.6Ca0.4CoO3 for bi-functional catalysis in an alkaline electrolyte, Electrochemistry Communications, 13 (2011) 321-324.

[93] Y. Zhu, S. Murali, W. Cai, X. Li, J.W. Suk, J.R. Potts, R.S. Ruoff, Graphene and graphene oxide: synthesis, properties, and applications, Advanced Materials, 22 (2010) 3906-3924.

[94] Z. Chen, W. Ren, B. Liu, L. Gao, S. Pei, Z.-S. Wu, J. Zhao, H.-M. Cheng, Bulk growth of mono-to few-layer graphene on nickel particles by chemical vapor deposition from methane, Carbon, 48 (2010) 3543-3550.

[95] A. Weidenkaff, S.G. Ebbinghaus, T. Lippert, Ln1-xAxCoO3 (Ln = Er, La; A = Ca, Sr)/Carbon Nanotube Composite Materials Applied for Rechargeable Zn/Air Batteries, Chemistry of Materials, 14 (2002) 1797-1805.

[96] D.C. Marcano, D.V. Kosynkin, J.M. Berlin, A. Sinitskii, Z. Sun, A. Slesarev, L.B. Alemany, W. Lu, J.M. Tour, Improved Synthesis of Graphene Oxide, ACS Nano, 4 (2010) 4806-4814.

[97] G.-Q. Zhang, X.-G. Zhang, H.-L. Li, Self-assembly preparation of mesoporous hollow nanospheric manganese dioxide and its application in zinc-air battery, J Solid State Electrochem, 10 (2006) 995-1001.

[98] D. Thiele, A. Züttel, Electrochemical characterisation of air electrodes based on La0.6Sr0.4CoO3 and carbon nanotubes, Journal of Power Sources, 183 (2008) 590-594.

[99] Z. Chen, A. Yu, R. Ahmed, H. Wang, H. Li, Z. Chen, Manganese dioxide nanotube and nitrogen-doped carbon nanotube based composite bifunctional catalyst for rechargeable zinc-air battery, Electrochimica Acta, 69 (2012) 295-300.

[100] H. Wang, Y. Yang, Y. Liang, G. Zheng, Y. Li, Y. Cui, H. Dai, Rechargeable Li-O2 batteries with a covalently coupled MnCo2O4-graphene hybrid as an oxygen cathode catalyst, Energy & Environmental Science, 5 (2012) 7931-7935.

[101] Z. Chen, D. Higgins, A. Yu, L. Zhang, J. Zhang, A review on non-precious metal electrocatalysts for PEM fuel cells, Energy & Environmental Science, 4 (2011) 3167-3192.

[102] D. Thiele, A. Züttel, Electrochemical characterisation of air electrodes based on la 0.6Sr0.4CoO3 and carbon nanotubes, Journal of Power Sources, 183 (2008) 590-594.

[103] K. Balasubramanian, M. Burghard, Chemically Functionalized Carbon Nanotubes, Small, 1 (2005) 180-192.

Appendix: Material Safety Data Sheet

The material safety data sheets of the following chemicals can be found from the manufacturer's website:

Carbon nanofibre, Vulcan carbon, potassium permanganate, potassium hydroxide, sodium hydroxide, ammonia gas, argon gas, ammonia hydroxide, sodium nitrate, cobalt nitrate hexhydrate, lanthanum nitrate hexhydrate, nickel nitrate hexhydrate, cobalt acetate tetrahydrate, hydrochloric acid, citric acid, phosphoric acid, sulfuric acid, nitric acid and Nafion.

Material Safety Data Sheet of Multi-walled Carbon Nanotubes

1. Product and Company Identification

Product name: Catalytic MWNT

Catalog #: MRCMW

Company: MER Corporation

7960 South Kolb Road, Tucson, Arizona 85706

Phone: (520)574-1980

Fax: (520)574-1983

2. Hazards identification

WHMIS Classification

D2B Toxic Material Causing Other Toxic Effects

Moderate respiratory irritant

Moderate eye irritant

HMIS Classification

Health hazard: 2

Flammability: 0

Physical hazards: 0

Potential health effects

Inhalation May be harmful if inhaled. Cause respiratory tract irritation.

Skin May be harmful if absorbed through skin. Causes skin irritation.

Eyes Causes eye irritation.

Ingestion May be harmful if swallowed.

3. First aid measures

General advice

Consult a physician. Show this safety data sheet to the doctor in attendance.Move out of dangerous area.

If inhaled

If breathed in, move person into fresh air. If not breathing, give artificial respiration. Consult a physician.

In case of skin contact

Wash off with soap and plenty of water. Consult a physician.

In case of eye contact

Rinse thoroughly with plenty of water for at least 15 minutes and consult a physician.

If swallowed

Never give anything by mouth to an unconscious person. Rinse mouth with water. Consult a physician.

4. Firefighting measures

Conditions of flammability

Not flammable or combustible.

Suitable extinguishing media

Use water spray, alcohol-resistant foam, dry chemical or carbon dioxide.

Special protective equipment for firefighters

Wear self-contained breathing apparatus for firefighting if necessary.

Hazardous combustion products

Hazardous decomposition products formed under fire conditions. - Carbon oxides

5. Accidental release measures

Personal precautions

Use personal protective equipment. Avoid dust formation. Avoid breathing vapors, mist or gas. Ensure adequate ventilation. Evacuate personnel to safe areas. Avoid breathing dust.

Environmental precautions

Do not let product enter drains.

Methods and materials for containment and cleaning up

Pick up and arrange disposal without creating dust. Sweep up and shovel. Keep in suitable, closed containers for disposal.

6. Handling and storage

Precautions for safe handling

Avoid contact with skin and eyes. Avoid formation of dust and aerosols. Provide appropriate exhaust ventilation at places where dust is formed.

Conditions for safe storage

Keep container tightly closed in a dry and well-ventilated place.

7. Expose control/personal protection

Contain no substances with occupational exposure limit values.

Personal protective equipment:

Respiratory protection

For nuisance exposures use particle respirator.

Use respirators and components tested and approved under appropriate government standards

Hand protection

Handle with gloves. Gloves must be inspected prior to use. Use proper glove removal technique (without touching glove's outer surface) to avoid skin contact with this product. Dispose of contaminated gloves after use in accordance with applicable laws and good laboratory practices. Wash and dry hands.

Eye protection

Safety glasses with side-shields. Use equipment for eye protection tested and approved under appropriate government standards.

Skin and body protection

The type of protective equipment must be selected according to the concentration and amount of the dangerous substance at the specific workplace.

Hygiene measures

Handle in accordance with good industrial hygiene and safety practice. Wash hands before breaks and at the end of workday.

Specific engineering controls

Use mechanical exhaust or laboratory fumehood to avoid exposure.